Quaternary Science Reviews 82 (2013) 104–120

Contents lists available at ScienceDirect

Quaternary Science Reviews

journal homepage: www.elsevier.com/locate/quascirev

Mid-Holocene net precipitation changes over China: model–data comparison

Dabang Jiang [a,b,c,*], Zhiping Tian [a,d], Xianmei Lang [e]

[a] Nansen-Zhu International Research Centre, Institute of Atmospheric Physics, Chinese Academy of Sciences, P.O. Box 9804, Beijing 100029, China
[b] Key Laboratory of Regional Climate–Environment Research for Temperate East Asia, Chinese Academy of Sciences, P.O. Box 9804, Beijing 100029, China
[c] Climate Change Research Center, Chinese Academy of Sciences, P.O. Box 9804, Beijing 100029, China
[d] University of Chinese Academy of Sciences, Beijing 100049, China
[e] International Center for Climate and Environment Sciences, Institute of Atmospheric Physics, Chinese Academy of Sciences, P.O. Box 9804, Beijing 100029, China

ARTICLE INFO

Article history:
Received 18 December 2012
Received in revised form
15 October 2013
Accepted 16 October 2013
Available online

Keywords:
Mid-Holocene
Net precipitation
Model–data comparison
Climate model
China

ABSTRACT

Many efforts have been made to reconstruct the moisture conditions over China during the mid-Holocene, approximately 6000 calendar years ago. However, most of them have been performed at the single site level or local scale, and the nationwide distribution of the mid-Holocene precipitation and net precipitation (precipitation minus evaporation) changes from both proxy data and simulations remains unclear. Here we first selected 36 out of 51 climate models participating in the Paleoclimate Modeling Intercomparison Project (PMIP) for their demonstrable ability to simulate the baseline climate and for the availability of evaporation data. Our analysis of the ensemble mean results of the 36 models shows that the mid-Holocene annual precipitation, evaporation, and net precipitation were 3.0%, 0.9%, and 6.9% more than the baseline period, respectively, and seasonally all three variables decreased in boreal winter and spring but increased in boreal summer and autumn on the national scale. For that period, both the pattern and magnitude of the above changes differed between the models and the sub-regions, and the interactive ocean effect had little impact overall on the country. Compared with the wetter-than-present climates derived from the records at 64 out of 69 sites across China, the models agreed qualitatively with the multi-proxy data in most parts of China, except Xinjiang and the areas between the middle and lower reaches of the Yangtze and Yellow River valleys, where drier-than-baseline climates were obtained from the 36 models.

© 2013 Elsevier Ltd. All rights reserved.

1. Introduction

Short instrumental records hamper our knowledge of climate change on decadal and longer timescales. Insights into the facts and mechanisms of past climate and environmental changes are thus essential for better understanding present and future climates. The mid-Holocene is a well-known period approximately 6000 years before present when the climate and environment differed from the present day, and it provides an excellent opportunity to examine how the climate system responds to changes in the latitudinal and seasonal distribution of insolation due to orbital forcing. In recent decades, considerable effort has been dedicated to the synthesis of proxy data and simulations as well as model–data comparisons for the mid-Holocene worldwide (e.g., Joussaume and Taylor, 1995; Guiot et al., 1999; Tarasov et al., 1999; Masson-Delmotte et al., 2006; Peyron et al., 2006; Braconnot et al., 2007; Zhang et al., 2010). It has been found that climate models are able to reproduce many of the robust qualitative large-scale features of reconstructed climate change, consistent with the understanding of orbital forcing (Jansen et al., 2007). On the regional scale, however, simulations have been found to be opposite the reconstructions of annual and winter (December–January–February) temperature changes in China (Jiang et al., 2012). An unresolved question at this stage is how the mid-Holocene moisture conditions are derived from both climate models and single-site-based proxy data over the country.

Using individual climate models of different complexities, several numerical experiments have been undertaken to address the mid-Holocene climate over China (Wang, 1999, 2000, 2002; Chen et al., 2002; Wei and Wang, 2004; Zheng et al., 2004; Zheng

* Corresponding author. Nansen-Zhu International Research Centre, Institute of Atmospheric Physics, Chinese Academy of Sciences, P.O. Box 9804, Beijing 100029, China. Tel.: +86 1082995229.
E-mail address: jiangdb@mail.iap.ac.cn (D. Jiang).

0277-3791/$ – see front matter © 2013 Elsevier Ltd. All rights reserved.
http://dx.doi.org/10.1016/j.quascirev.2013.10.017

Table 1
Basic information on the general circulation models used in the present study.

Model ID		Project	Atmospheric resolution	Length of run analyzed (year)	Baseline period
01	CCC2.0	PMIP1 (AGCM)	T32L10	10	Modern
02	CCM3	PMIP1 (AGCM)	T42L18	8	Modern
03	CCSR1	PMIP1 (AGCM)	T21L20	10	Modern
04	CNRM-2	PMIP1 (AGCM)	T31L19	10	Modern
05	CSIRO	PMIP1 (AGCM)	R21L9	15	Modern
06	ECHAM3	PMIP1 (AGCM)	T42L19	10	Modern
07	GEN2	PMIP1 (AGCM)	T31L18	10	Modern
08	GFDL	PMIP1 (AGCM)	R30L20	25	Modern
09	GISS-IIP	PMIP1 (AGCM)	72 × 46, L9	10	Modern
10	LMCELMD4	PMIP1 (AGCM)	48 × 36, L11	15	Modern
11	LMCELMD5	PMIP1 (AGCM)	64 × 50, L11	15	Modern
12	MRI2	PMIP1 (AGCM)	72 × 46, L15	10	Modern
13	UGAMP	PMIP1 (AGCM)	T42L19	20	Modern
14	UIUC11	PMIP1 (AGCM)	72 × 46, L14	10	Modern
15	UKMO	PMIP1 (AGCM)	96 × 73, L19	50	Modern
16	YONU	PMIP1 (AGCM)	72 × 46, L7	10	Modern
17	CCSM3.0	PMIP2 (AOGCM)	T42L18	50	Pre-industrial
18	CSIRO-Mk3L-1.0	PMIP2 (AOGCM)	R21L18	1000	Pre-industrial
19	CSIRO-Mk3L-1.1	PMIP2 (AOGCM)	R21L18	1000	Pre-industrial
20	ECBILTCLIOVECODE	PMIP2 (AOGCM)	T21L3	100	Pre-industrial
21	ECHAME5-MPIOM1	PMIP2 (AOGCM)	T31L20	100	Pre-industrial
22	ECHAM53-MPIOM127-LPJ	PMIP2 (AOGCM)	T31L19	100	Pre-industrial
23	FGOALS-1.0 g	PMIP2 (AOGCM)	R42L9	100	Pre-industrial
24	FOAM	PMIP2 (AOGCM)	R15L18	100	Pre-industrial
25	GISSmodelE	PMIP2 (AOGCM)	72 × 46, L17	50	Pre-industrial
26	IPSL-CM4-V1-MR	PMIP2 (AOGCM)	96 × 72, L19	100	Pre-industrial
27	MIROC3.2	PMIP2 (AOGCM)	T42L20	100	Pre-industrial
28	MRI-CGCM2.3.4fa	PMIP2 (AOGCM)	T42L30	150	Pre-industrial
29	MRI-CGCM2.3.4nfa	PMIP2 (AOGCM)	T42L30	150	Pre-industrial
30	UBRIS-HadCM3M2	PMIP2 (AOGCM)	96 × 73, L19	100	Pre-industrial
31	ECBILTCLIOVECODE-veg	PMIP2 (AOVGCM)	T21L3	100	Pre-industrial
32	ECHAM53-MPIOM127-LPJ-veg	PMIP2 (AOVGCM)	T31L19	100	Pre-industrial
33	FOAM-veg	PMIP2 (AOVGCM)	R15L18	100	Pre-industrial
34	MRI-CGCM2.3.4fa-veg	PMIP2 (AOVGCM)	T42L30	100	Pre-industrial
35	MRI-CGCM2.3.4nfa-veg	PMIP2 (AOVGCM)	T42L30	100	Pre-industrial
36	UBRIS-HadCM3M2-veg	PMIP2 (AOVGCM)	96 × 73, L19	100	Pre-industrial
37	BCC-CSM1.1	PMIP3 (AOVGCM)	T42L26	100	Pre-industrial
38	CCSM4	PMIP3 (AOGCM)	288 × 192, L26	301	Pre-industrial
39	CNRM-CM5	PMIP3 (AOGCM)	256 × 128, L31	200	Pre-industrial
40	CSIRO-Mk3-6-0	PMIP3 (AOGCM)	192 × 96, L18	100	Pre-industrial
41	CSIRO-Mk3L-1-2	PMIP3 (AOGCM)	64 × 56, L18	500	Pre-industrial
42	EC-EARTH-2-2	PMIP3 (AOGCM)	320 × 160, L62	40	Pre-industrial
43	FGOALS-g2	PMIP3 (AOVGCM)	128 × 60, L26	100	Pre-industrial
44	FGOALS-s2	PMIP3 (AOVGCM)	128 × 108, L26	100	Pre-industrial
45	GISS-E2-R	PMIP3 (AOGCM)	144 × 90, L40	100	Pre-industrial
46	HadGEM2-CC	PMIP3 (AOVGCM)	192 × 145, L60	35	Pre-industrial
47	HadGEM2-ES	PMIP3 (AOVGCM)	192 × 145, L38	102	Pre-industrial
48	IPSL-CM5A-LR	PMIP3 (AOVGCM)	96 × 95, L39	500	Pre-industrial
49	MIROC-ESM	PMIP3 (AOVGCM)	T42L80	100	Pre-industrial
50	MPI-ESM-P	PMIP3 (AOGCM)	T63L47	100	Pre-industrial
51	MRI-CGCM3	PMIP3 (AOGCM)	320 × 160, L48	100	Pre-industrial

and Yu, 2009; Zhou and Zhao, 2010; Liu et al., 2010a). They have well explained the increase of surface temperature and the intensification of monsoon, as suggested by proxy data, over China during the mid-Holocene summer (June–July–August). At the same time, these experiments have shown a large inter-model spread in the magnitude and sign of the mid-Holocene precipitation changes. Among these simulations, for example, the mid-Holocene summer precipitation increased consistently over eastern China (Wang, 1999), while it increased in southern and northeastern China but decreased in central and northern China (Zheng and Yu, 2009). For that period, the annual precipitation increased over western China, northern China, and most parts of southern China, but decreased in the middle and lower reaches of the Yangtze River valley and coastal southern China (Zheng et al., 2004), while large orbital-induced variations of annual precipitation occurred only in northeastern China (Liu et al., 2010a). Such model-dependent uncertainties make it of particular interest to integrate the outputs of multiple climate models to analyze the similarities and differences between the model results of precipitation. Next, dynamic ocean and vegetation are two key components of the climate system, and their effects have been identified as important for the mid-Holocene climate (e.g., Kutzbach et al., 1996; Ganopolski et al., 1998; Zhao et al., 2005; Braconnot et al., 2007; Jansen et al., 2007; Dallmeyer et al., 2010). However, these components have not or have only been partly taken into account in the aforementioned experiments with atmospheric general circulation models (AGCMs) (Wang, 1999, 2000, 2002; Chen et al., 2002), regional climate models nested within AGCMs (Zheng et al., 2004; Liu et al., 2010a), an asynchronously coupled atmosphere–ocean general circulation model (Wei and Wang, 2004), and fully coupled

atmosphere–ocean general circulation models (AOGCMs) (Zheng and Yu, 2009; Zhou and Zhao, 2010). It remains unclear how annual and seasonal precipitation and evaporation over China respond to the mid-Holocene orbital forcing and slight changes in atmospheric concentrations of greenhouse gases in the simulations of current AOGCMs and fully coupled atmosphere–ocean–vegetation general circulation models (AOVGCMs). Hereafter AOGCMs plus AOVGCMs are referred to as coupled general circulation models (CGCMs).

Based on a great deal of reconstruction work, it has been proposed that the regional climate of China underwent generally wetter conditions during the mid-Holocene (see Section 4 of this study). Those proxy data form a solid foundation for qualitative model–data comparisons of the moisture conditions over the country. The question then arises as to the extent to which reconstructions are compatible with available simulations over China. Note that unlike the previous few model–data comparisons based on individual model results and limited records (Wang, 1999; Chen et al., 2002; Zheng et al., 2004; Liu et al., 2010a), comparisons between multiple climate models and multiple proxy data are more helpful for examining the nature and cause of the mid-Holocene climate change. Previously, the increase of the mid-Holocene summer precipitation was obtained by 12 CGCMs within the Paleoclimate Modeling Intercomparison Project (PMIP) phase 2 (PMIP2), and it was found to generally agree with annually resolved records at 24 sites over China (Wang et al., 2010a). However, a fair model–data comparison should be annual vs. annual rather than summer vs. annual, while reconstructed moisture conditions should be compared directly with changes in net precipitation (precipitation minus evaporation) rather than indirectly with precipitation, as evaporation is a key variable for moisture. In addition, in the work of Wang et al. (2010a) there was quite a limited number and an uneven geographical distribution of proxy data sites over China; only part of the PMIP2 CGCMs were used; and a previous generation of climate models that participated in the PMIP phase 1 (PMIP1) were not included, so it is impossible to evaluate the role of an interactive ocean through the comparison of different types of PMIP simulations.

Taken together, an analysis is made in this paper of the mid-Holocene net precipitation changes over China from the perspective of multiple and reliable climate models and proxy data. The key questions for the mid-Holocene are (1) how annual and seasonal precipitation, evaporation, and net precipitation changed over China, (2) whether there was a detectable interactive ocean effect on moisture conditions over the country, and (3) the extent to which simulations are compatible with proxy data.

2. Data

2.1. Model, reanalysis, and proxy data

This study was based on all available simulations for the mid-Holocene climate under the framework of the PMIP at the moment, including experiments using 16 AGCMs in the PMIP1, 20 CGCMs in the PMIP2, and 15 CGCMs in the PMIP phase 3 (PMIP3) within the framework of the Coupled Model Intercomparison Project phase 5 (CMIP5). For the mid-Holocene experiment, the core forcing lies in orbitally induced changes of ~5% in the seasonal distribution of the incoming solar radiation at the top of the atmosphere in the Northern and Southern Hemispheres (Berger, 1978). In addition, the atmospheric CO_2 concentration was set to 280 ppm for the mid-Holocene instead of 345 ppm in 1985 for the modern (baseline) period in the PMIP1. The atmospheric CO_2 concentration was held constant at 280 ppm, and the atmospheric CH_4 concentration was set to 760 ppb for the pre-industrial (baseline) period and 650 ppb for the mid-Holocene in the PMIP2. In the PMIP3, the atmospheric concentrations of CO_2, CH_4, and N_2O varied from the pre-industrial levels of 284 ppm, 791 ppb, and 275 ppb to 280 ppm, 650 ppb, and 270 ppb during the mid-Holocene, respectively. For both the baseline and mid-Holocene experiments, sea surface temperatures were fixed at the present values in AGCMs but were simulated by oceanic general circulation models in CGCMs, and the vegetation was simulated by equilibrium or dynamic global vegetation models in AOVGCMs but was fixed at the present vegetation in the other models. The outputs of 51 climate models were provided by international modeling groups and were archived in the PMIP and/or CMIP5 database from which we downloaded the data of concern. Basic information on the models and data is provided in Table 1. More details were given by Joussaume and Taylor (1995) and Braconnot et al. (2007) and are available online at http://pmip.lsce.ipsl.fr/and http://cmip-pcmdi.llnl.gov/cmip5/.

The reanalysis data used to assess the ability of the models to simulate the baseline annual precipitation climatology over China were the long-term mean precipitation taken from the CPC Merged Analysis of Precipitation (CMAP) for the period 1979–2000 (Xie and Arkin, 1997). These data were provided by the NOAA/OAR/ESRL PSD, Boulder, Colorado, USA, from their website at http://www.esrl.noaa.gov/psd. Considering that atmospheric horizontal resolution differs from model to model, all model and reanalysis data were aggregated to a relatively mid-range resolution of 96 × 48 (longitude × latitude, an equivalent grid spacing of roughly 3.75° × 3.75°). The ensemble mean of multiple climate models was obtained with the same weights across the models of analysis.

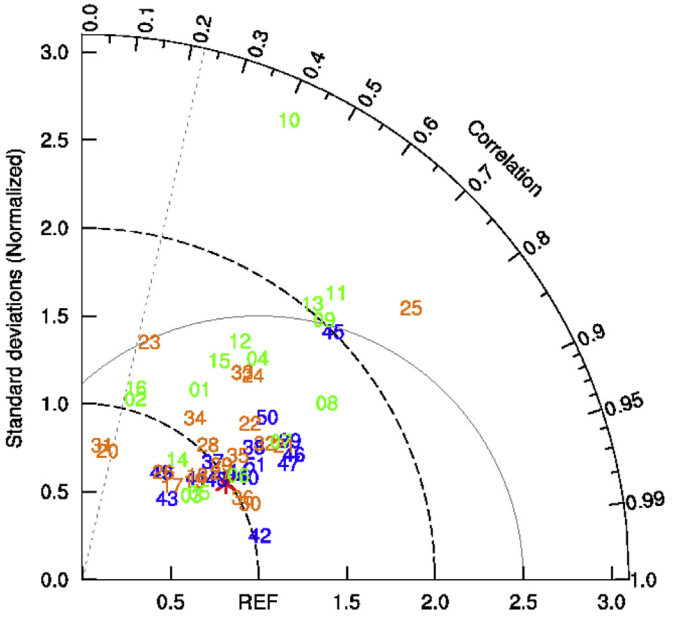

Fig. 1. Taylor diagram (Taylor, 2001) for displaying normalized pattern statistics of climatological annual precipitation over China between the 51 PMIP models for the baseline period and the CMAP data for the period 1979–2000 (Xie and Arkin, 1997). Each number represents a Model ID (See Table 1); green, orange, and blue represent the PMIP1, PMIP2, and PMIP3 models, respectively; red star represents the ensemble mean of the 36 models chosen for analysis; and the CMAP is considered as the reference (REF). The standard deviation and CRMSD are normalized by the CMAP standard deviation. The radial distance from the origin is the normalized standard deviation of a model; the SCC between a model and the reference is given by the azimuthal position of the model, with oblique dotted line showing the 95% confidence level; and the normalized CRMSD between a model and the reference is their distance apart. (For interpretation of the references to color in this figure legend, the reader is referred to the web version of this article.)

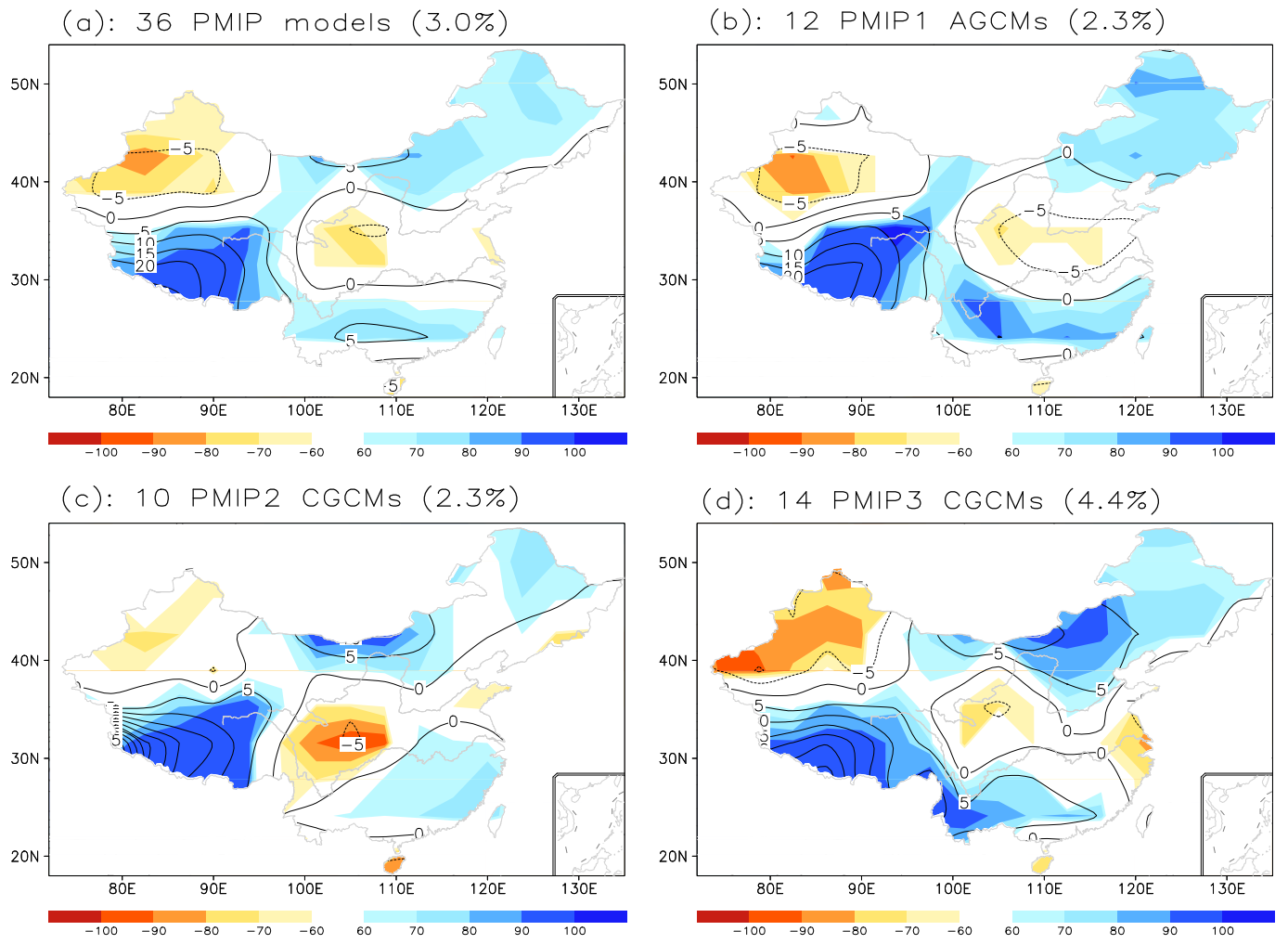

Fig. 2. Percentage changes in annual precipitation (contour, units: %) during the mid-Holocene, with reference to the baseline period, for the ensemble mean of the (a) 36 PMIP models, (b) 12 PMIP1 AGCMs, (c) 10 PMIP2 CGCMs, and (d) 14 PMIP3 CGCMs. In each panel, the consistency index of the models (units: %) in simulating the direction of the changes (namely, the percentage of the number of models agreeing on the sign of the change according to the algorithm of Wang (2005), the same below) in annual precipitation is shown in shading, and regionally averaged change in China is given in parentheses.

The proxy data used to compare the model results were reconstructions of the mid-Holocene precipitation and/or moisture changes over China. These data were mostly expressed in a qualitative manner and were composed of records of ice cores, lake cores, palaeosols, peat, pollen, sediments, and stalagmites at 74 sites across the country. All these data and the corresponding references are detailed in the model–data comparison in Section 4.

2.2. Evaluation of 51 PMIP climate models

Whether climate models can reliably reproduce the geographical distribution, magnitude, and spatial variability of the baseline period annual precipitation climatology over China determines the confidence of their results for the mid-Holocene. Therefore, based on 77 grid points across the Chinese mainland, spatial correlation coefficients (SCCs) between the CMAP data and baseline simulations were calculated model by model, as was the standard deviation and centered root mean square difference (CRMSD) of each baseline simulation with respect to the CMAP data. The SCCs were used to quantify the similarity between simulated and observed spatial patterns, and the normalized standard deviation and CRMSD by the CMAP standard deviation were used to measure the spatial variability and internal model error of the models, respectively. The Taylor diagram in Fig. 1 shows that the SCCs ranged from 0.13 to 0.97; the normalized standard deviations ranged from 0.67 to 2.86; and the normalized CRMSDs ranged from 0.26 to 2.62. These values indicate that the abilities of the models differed from one another, and some models failed to simulate the basic features of the observed annual precipitation climatology for the baseline period. Accordingly, four thresholds were arbitrarily set to identify reliable climate models. First, the SCC had to be positive and statistically significant at the 95% confidence level, namely, larger than 0.23; second, the normalized standard deviation had to be larger than 0.5 and less than 2.0; third, the normalized CRMSD had to be less than 1.5; and fourth, evaporation data had to be available, as they are necessary for calculating net precipitation. In this manner, 12, 10, and 14 models were finally chosen from the 16 PMIP1, 20 PMIP2, and 15 PMIP3 models for analysis based on the results presented in Fig. 1, respectively. Note that the SCCs were 0.77, 0.72 and 0.89, while the normalized CRMSDs were

0.68, 0.77, and 0.46 for the ensemble mean of the 12 PMIP1, 10 PMIP2, and 14 PMIP3 models, respectively, indicating an overall better performance for the PMIP3 models compared with the previous generations of climate models. In addition, the ensemble mean of all 36 chosen models gave an SCC of 0.83, a normalized standard deviation of 0.98, and a normalized CRMSD of 0.58; hence, it had a higher reliability with reference to most of the individual models (Fig. 1). The ensemble mean of the results of the 36 models was therefore emphasized in our analysis. MME-PMIP1, MME-PMIP2, MME-PMIP3, and MME-PMIP are hereafter denoted as the ensemble mean of the 12 PMIP1 AGCMs, 10 PMIP2 CGCMs, 14 PMIP3 CGCMs, and all 36 PMIP models, respectively.

3. Mid-Holocene precipitation, evaporation, and net precipitation changes over China from PMIP simulations

3.1. Precipitation

In response to the mid-Holocene forcing, the annual precipitation varied from −10% to 25% over China and increased in 64% of the area of the country with respect to the baseline period according to MME-PMIP (Fig. 2a). The annual precipitation decreased in Xinjiang and the areas between the middle and lower reaches of the Yangtze and Yellow River valleys, but increased in the rest of the country, particularly on the Qinghai-Tibetan Plateau, where the greatest increase was up to 25%. Moreover, most of these changes were consistent among the models, which were measured by a consistency index defined as the percentage of the number of models agreeing on the sign of the change (Wang, 2005). Averaged across the whole country and the 36 PMIP models, the mid-Holocene annual precipitation was 3.0% greater than that of the baseline period.

The models differed somewhat from one another in the mid-Holocene annual precipitation changes (Fig. 3a). Averaged over China, the annual precipitation increased in 31 of the 36 PMIP models but decreased in the remaining five models. As introduced previously, AGCMs were used in the PMIP1, and CGCMs were used in the PMIP2 and PMIP3, allowing for a preliminary evaluation of the interactive ocean effect. When viewed in terms of these two types of climate models from the perspective of the whole country, the annual precipitation increased in 11 of the 12 PMIP1 AGCMs and 20 of the 24 PMIP2 and PMIP3 CGCMs. The MME-PMIP1 reproduced a country-average increase of 2.3%, which was the same as that of the MME-PMIP2 and nearly 4.4% of the MME-PMIP3. Moreover, like the spatial pattern of the MME-PMIP (Fig. 2a), the geographical distribution of large-scale annual precipitation change was consistent between the AGCMs and CGCMs (Fig. 2b–d). All these results indicate that the interactive ocean effect had little impact on annual precipitation over China as a whole during the mid-Holocene. Regionally, there existed differences among the PMIP1, PMIP2, and PMIP3 groups of the models. For instance, the decreased annual precipitation in Xinjiang and the increased annual precipitation in northern China were more marked in the PMIP3 models (Fig. 2d) than in the PMIP1 and PMIP2 models (Fig. 2b–c) in terms of both magnitude and consistency. Such discrepancies should be related to the differences in the physics and dynamics of the models, the boundary conditions, and the experimental designs.

On the seasonal scale, the mid-Holocene precipitation changes differed largely from the above annual results (Fig. 3b–e and 4). In winter, all 36 models reproduced less than baseline precipitation, with an average of −8.2%, −11.9%, −10.0%, and −9.9% for MME-PMIP1, MME-PMIP2, MME-PMIP3, and MME-PMIP, respectively (Fig. 3b). Spatially, the MME-PMIP

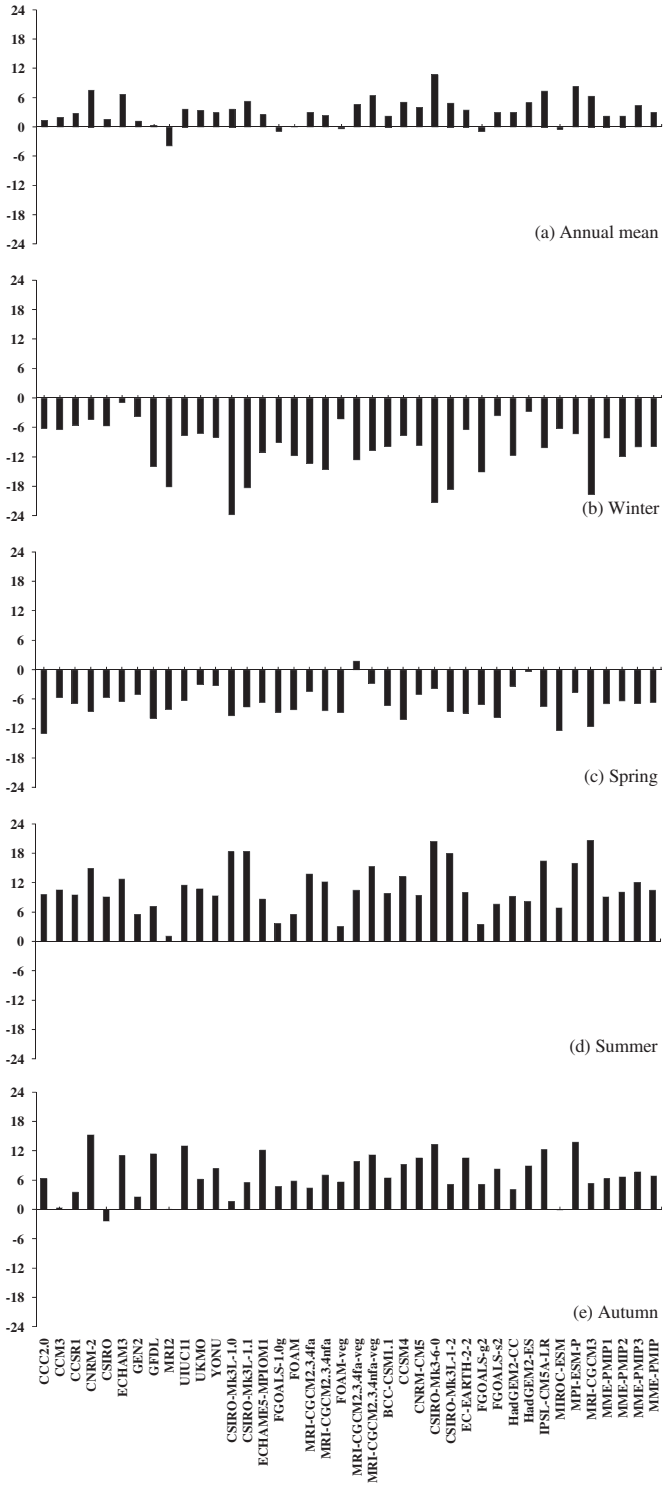

Fig. 3. Percentage changes in regionally averaged annual and seasonal precipitation (units: %) over China during the mid-Holocene with respect to the baseline period.

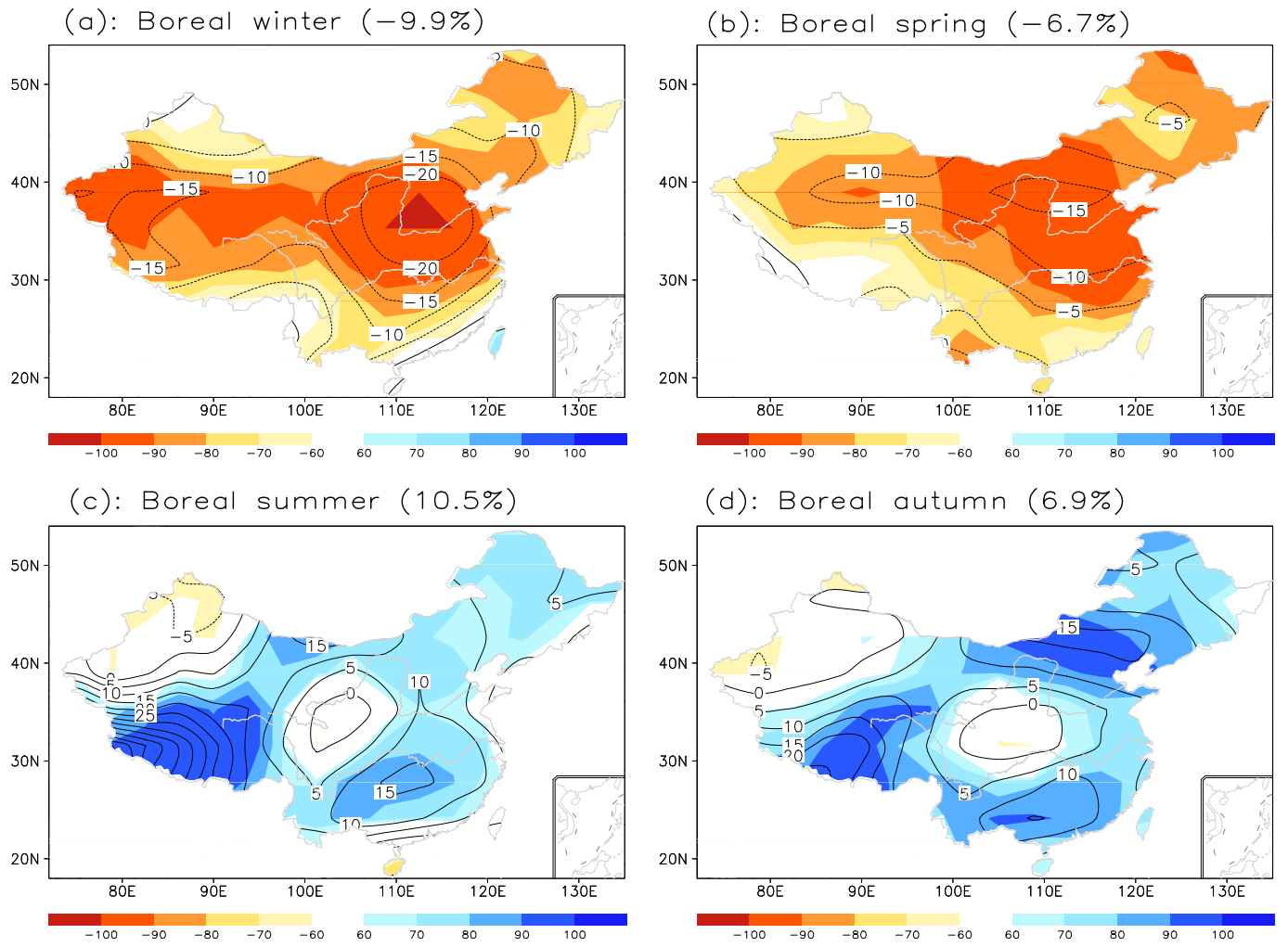

Fig. 4. Percentage changes in seasonal precipitation (contour, units: %) during the mid-Holocene, with reference to the baseline period, for the ensemble mean of the 36 PMIP models. In each panel, the consistency index of the models (units: %) in simulating the direction of the changes in seasonal precipitation is shown in shading, and regionally averaged change in China is given in parentheses.

precipitation decreased by 0–25% over China and by more than 10% over the region of approximately 30°–45°N, particularly in the middle and lower reaches of the Yangtze and Yellow River valleys (Fig. 4a). This large-scale precipitation decrease in eastern China was related to the strengthening of the mid-Holocene East Asian winter monsoon. It can be observed in Fig. 5a and c that anomalous northerly winds prevailed in eastern China due to orbitally induced increases in land–sea thermal contrasts and sea level pressure gradients between continental Asia and the western North Pacific. Accordingly, more cold and dry air from the high latitudes entered East Asia, suppressing the warm and moist air from the low latitudes. In turn, precipitation decreased in eastern China. In fact, this reverse relationship between the East Asian winter monsoon strength and precipitation in eastern China has been reported for the modern period (e.g., Wang and Chen, 2010). In spring (March–April–May), precipitation decreased in 35 of the 36 PMIP models (Fig. 3c), with an average of −6.9%, −6.4%, −6.8%, and −6.7% for the ensemble mean of PMIP1, PMIP2, PMIP3, and all PMIP models, respectively. In MME-PMIP, the geographical distribution of spring precipitation changes was generally similar to the above winter pattern, but with an overall smaller magnitude (Fig. 4b).

In summer, the mid-Holocene precipitation increased in all 36 PMIP models, averaging 9.2%, 10.1%, 12.1%, and 10.5% in MME-PMIP1, MME-PMIP2, MME-PMIP3, and MME-PMIP, respectively (Fig. 3d). Based on MME-PMIP, precipitation slightly decreased in central and northern Xinjiang and the region of approximately 30°–38°N and 98°–108°E, but increased in the rest of the country, particularly in most parts of the Qinghai-Tibetan Plateau, where the increase was more than 15% and up to 50% on its southern margin (Fig. 4c). Note that because summer precipitation accounts for more than half the total annual precipitation over China [for example, 55% for the modern period 1960–2009 (Sui et al., 2013)], the spatial pattern of summer precipitation change was generally similar to the annual result (Fig. 2a) over the country, except in the middle and lower reaches of the Yangtze and Yellow River valleys, where, as mentioned before, winter and spring precipitation decreased by more than 10%. In eastern China, the precipitation increase was closely related to a strengthened monsoon circulation during the mid-Holocene summer. Based on the ensemble mean of 35 of the

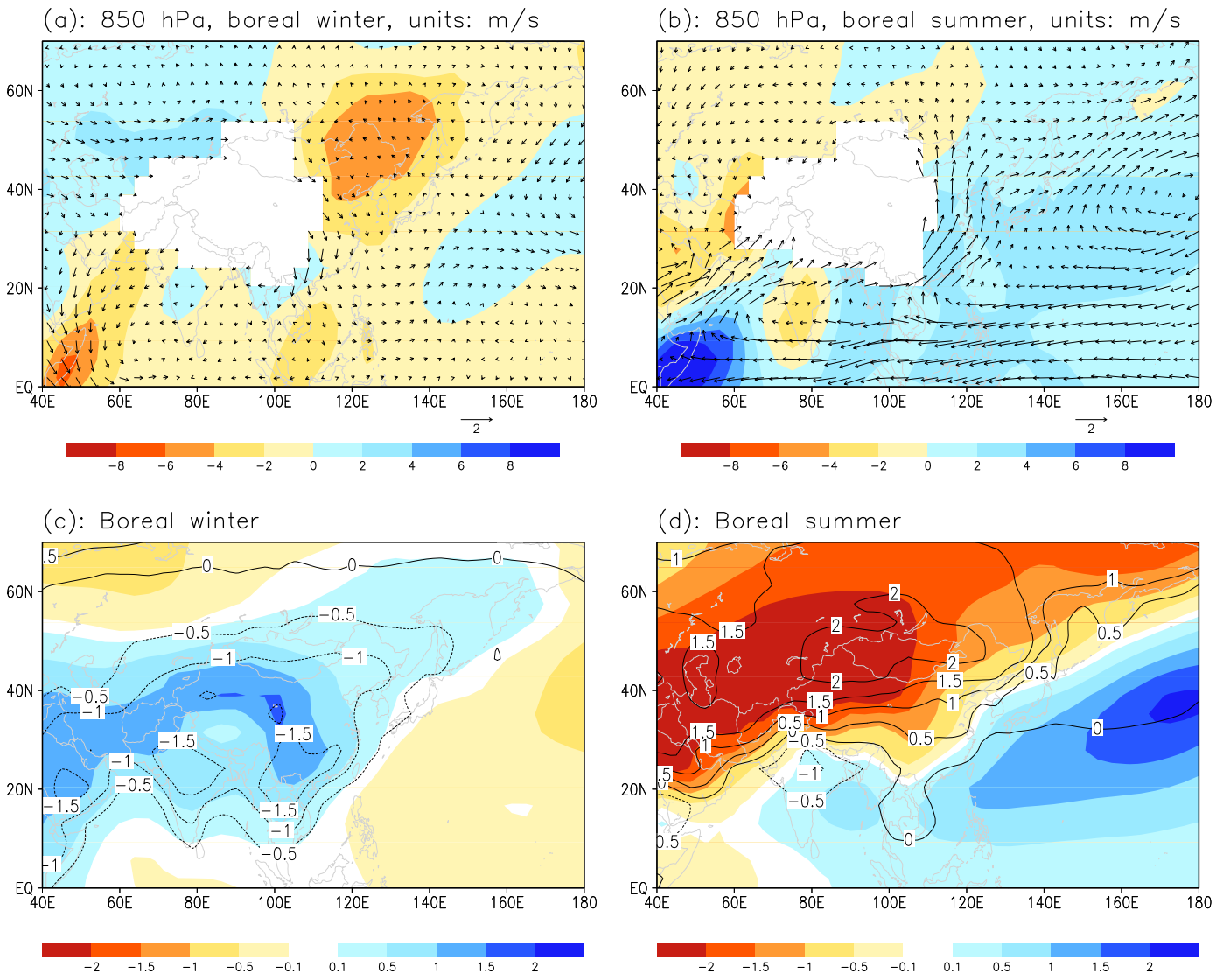

Fig. 5. Mid-Holocene–baseline anomalies of (a) winter and (b) summer winds, together with the baseline period meridional wind climatology (shading; northward wind speed is positive), for the ensemble mean of the 35 PMIP models (excluding EC-EARTH-2-2 for which wind data are not available), in which regions with an elevation above 1500 m are left blank. Also shown are the accompanying mid-Holocene–baseline anomalies of (c) winter and (d) summer surface air temperature (contour, units: K) and sea level pressure (shading, units: hPa).

36 PMIP models (excluding EC-EARTH-2-2 with wind data not available), anomalous southerly winds prevailed in the lower troposphere in East Asia during that period because of an enhanced land–sea thermal contrast and, hence, sea level pressure gradient between the East Asian continent and adjacent oceans as a result of orbital forcing (Fig. 5b and d). These changes are consistent with the results of the 28 PMIP models with a demonstrable ability to simulate the modern East Asian summer monsoon climatology (Jiang et al., 2013). In addition, for that period there was similar pattern and magnitude in large-scale summer precipitation changes in China between the results of MME-PMIP1 and MME-PMIP2 or MME-PMIP3, indicating little interactive ocean effect. This is generally in line with the multi-model result (Zhao and Harrison, 2012) but is in disagreement with the result of either positive (Wei and Wang, 2004) or negative (Liu et al., 2004; Marzin and Braconnot, 2009) effects obtained from individual models. In autumn (September–October–November), precipitation increased in 34 of the 36 PMIP models, with a nationwide average of 6.3%, 6.7%, 7.8%, and 6.9% for the ensemble mean of PMIP1, PMIP2, PMIP3, and all PMIP models, respectively (Fig. 3e). On the whole, the autumn precipitation changes in MME-PMIP were similar in distribution to the summer case, but with an overall smaller magnitude (Fig. 4d).

3.2. Evaporation

With reference to the baseline period, the mid-Holocene annual evaporation varied from −6% to 12% over China in MME-PMIP (Fig. 6a). The annual evaporation decreased in Xinjiang, southwestern China and coastal northern China but increased in the rest of the country, displaying a similar pattern to the annual precipitation changes in northern and western China (Fig. 2a). Meanwhile, the model agreements were higher than 60% in most parts of China, except central and southeastern China. On the national scale, the MME-PMIP annual evaporation increased by an average of 0.9%. For

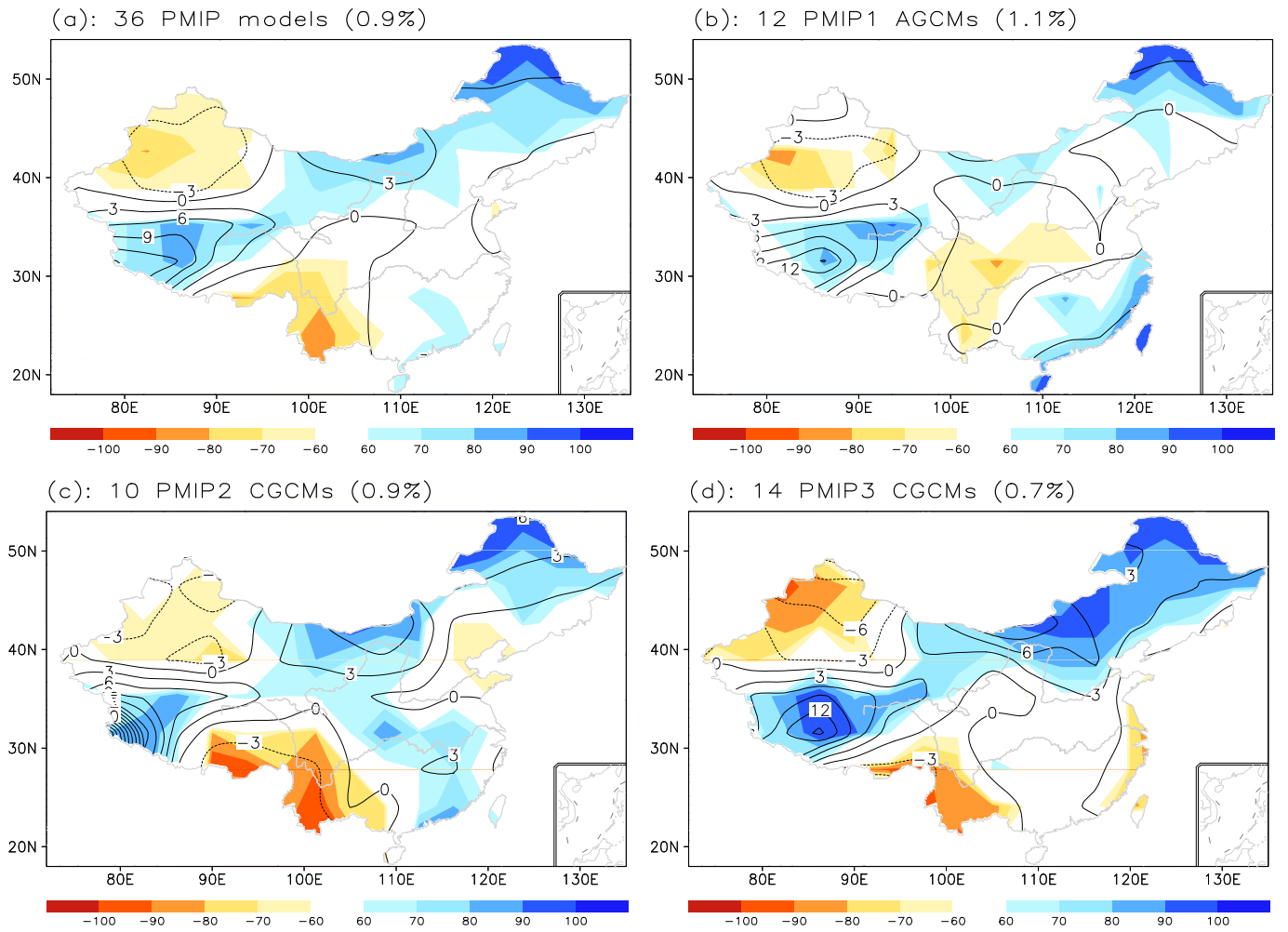

Fig. 6. Percentage changes in annual evaporation (contour, units: %) during the mid-Holocene, with reference to the baseline period, for the ensemble mean of the (a) 36 PMIP models, (b) 12 PMIP1 AGCMs, (c) 10 PMIP2 CGCMs, and (d) 14 PMIP3 CGCMs. In each panel, the consistency index of the models (units: %) in simulating the direction of the changes in annual evaporation is shown in shading, and regionally averaged change in China is given in parentheses.

individual models, the regionally averaged annual evaporation increased in 23 of the 36 PMIP models but decreased in the remaining 13 models (Fig. 7a). When viewed in terms of AGCMs and CGCMs, the annual evaporation increased by a similar magnitude for MME-PMIP1 (1.1%), MME-PMIP2 (0.9%), and MME-PMIP3 (0.7%). Moreover, the geographical distribution of large-scale annual evaporation change generally agreed among the three sets of experiments, although there were regional differences, such as larger and more consistent changes in Xinjiang, northern China, and the Qinghai-Tibetan Plateau in the PMIP3 models than in the PMIP1 and PMIP2 models (Fig. 6b–d). These results imply the interactive ocean effect on the mid-Holocene annual evaporation over China was limited as a whole.

On the seasonal scale, both the spatial pattern and magnitude of the mid-Holocene evaporation changes differed from the above annual results (Fig. 7b–e and 8). In winter, 31 of the 36 models reproduced less than baseline evaporation averaged over China during the mid-Holocene, with an average of −3.4%, −4.0%, −5.0%, and −4.1% for MME-PMIP1, MME-PMIP2, MME-PMIP3, and MME-PMIP, respectively (Fig. 7b). Based on MME-PMIP, winter evaporation decreased across almost the whole China, except coastal southeastern China, and by an overall larger magnitude in northern China (Fig. 8a). Like winter, all but one model reproduced less spring evaporation for that period compared with the baseline period, with a nationwide average of −4.1%, −5.3%, −5.1%, and −4.7% for the ensemble mean of PMIP1, PMIP2, PMIP3, and all PMIP models, respectively (Fig. 7c). The MME-PMIP spring evaporation was consistently reduced over China, except coastal southeastern China and southernmost Tibet (Fig. 8b). For both winter and spring, the mid-Holocene evaporation reduction was at least partly due to decreased precipitation (Fig. 4a–b) and temperature (Fig. 5c), as heat, humidity, and air movement are key factors influencing evaporation. Previously, winter and spring temperatures had been revealed to significantly decrease over China in response to a negative radiative forcing due to changes in the earth's orbital parameters and atmospheric concentrations of greenhouse gases (Jiang et al., 2012).

In the mid-Holocene summer, all but one model reproduced more evaporation averaged over China compared with the baseline period (Fig. 7d). Summer evaporation increased by 5.9%, 5.3%, 4.8%, and 5.4% for the ensemble mean of PMIP1, PMIP2, PMIP3, and all PMIP models, respectively. According to MME-PMIP, summer evaporation increased in almost the whole China, except in the east coastal region, southernmost Tibet, and central Xinjiang (Fig. 8c).

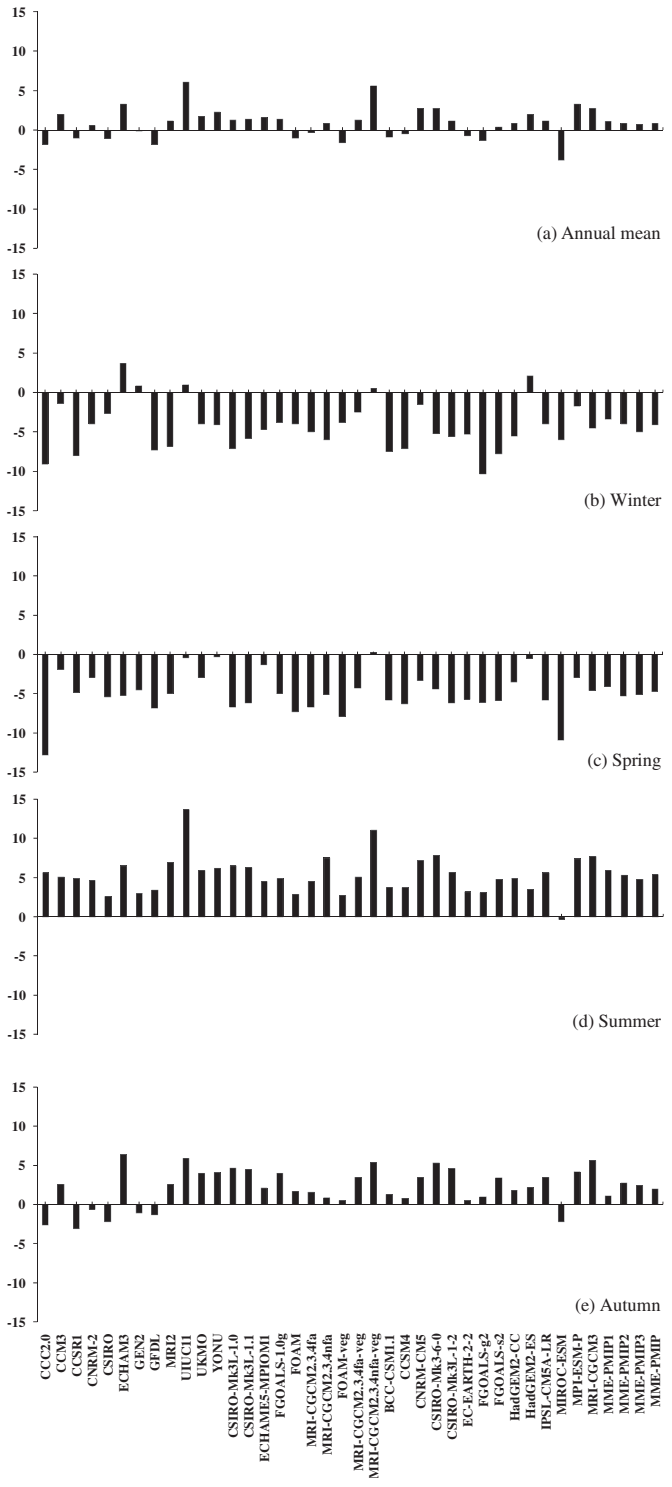

Fig. 7. Percentage changes in regionally averaged annual and seasonal evaporation (units: %) over China during the mid-Holocene with respect to the baseline period.

Such an evaporation increase was directly related to surface warming (Fig. 5d) due to an orbitally induced positive radiative forcing of 21.3 W m^{-2} averaged over China during the mid-Holocene summer (Jiang et al., 2012). In autumn, the mid-Holocene evaporation increased in 29 of the 36 PMIP models and by 1.1–2.8% for the ensemble mean of PMIP1, PMIP2, PMIP3, and all PMIP models (Fig. 7e). Interestingly, less than baseline autumn evaporation was reproduced by half the 12 PMIP1 AGCMs, but by only one of the 24 PMIP2 and PMIP3 CGCMs. This result was related to the difference in the mid-Holocene autumn temperature changes between the AGCMs and CGCMs. On the national scale, autumn temperature decreased in all 12 AGCMs but increased in most of the 24 CGCMs, which is in turn associated with a warming effect of interactive ocean on autumn temperature over the country as detailed in Jiang et al. (2012).

3.3. Net precipitation

Taking into account the above changes in both annual precipitation and evaporation, for that period, the regionally averaged annual net precipitation over China increased in 33 of the 36 PMIP models with reference to the baseline period (Fig. 9a). For the whole country, the mid-Holocene annual net precipitation increased on average by 4.6% or 0.05 mm/day for the 12 PMIP1 AGCMs, by 4.3% or 0.05 mm/day for the 10 PMIP2 CGCMs, by 11.9% or 0.09 mm/day for the 14 PMIP3 CGCMs, and by 6.9% or 0.06 mm/day for the 36 PMIP models. Based on MME-PMIP, the annual net precipitation decreased in Xinjiang but increased in the rest of western China west of approximately 100°E, while it decreased in northern Northeast China and the middle and lower reaches of the Yangtze and Yellow River valleys but increased in the rest of eastern China east of approximately 100°E (Fig. 10a). A comparable pattern and magnitude of the annual net precipitation changes between the AGCMs and CGCMs implies little interactive ocean effect on the mid-Holocene annual net precipitation over China (Fig. 10b–d). In addition, although the geographical distribution of the changes in the mid-Holocene annual precipitation and net precipitation was similar on the large scale, there were regional differences between the two due to annual evaporation changes (Figs. 2a, 6a and 10a). For example, more annual precipitation occurred in northern Northeast China, whereas more annual evaporation led to less annual net precipitation there. It is also noted that the area with more annual net precipitation accounted for 56% of the area of the country, which is less than the aforementioned 64% for annual precipitation according to MME-PMIP. These results show the limitation of previous studies comparing simulated precipitation changes directly with the moisture conditions suggested by proxy data (e.g., Wang, 1999; Chen et al., 2002; Zheng et al., 2004; Liu et al., 2010a).

The mid-Holocene net precipitation changes differed between the seasons (Fig. 9b–e and 11). All but two models (one model) reproduced less than baseline winter (spring) net precipitation, while all but one model (four models) reproduced more than baseline summer (autumn) net precipitation during the mid-Holocene. Averaged over the whole country and the 36 PMIP models, the net precipitation decreased by 10.0% or 0.08 mm/day in winter and by 10.1% or 0.11 mm/day in spring but increased by 18.6% or 0.33 mm/day in summer and by 20.4% or 0.12 mm/day in autumn. The aforementioned annual net precipitation increase was therefore derived from the greater net precipitation in summer and autumn due to a larger increase in precipitation than evaporation in both seasons. In addition, although there were regional differences in magnitude and sign, the spatial pattern of seasonal net precipitation changes was similar to that of seasonal precipitation changes (Figs. 4 and 11). For example, winter and spring net precipitation

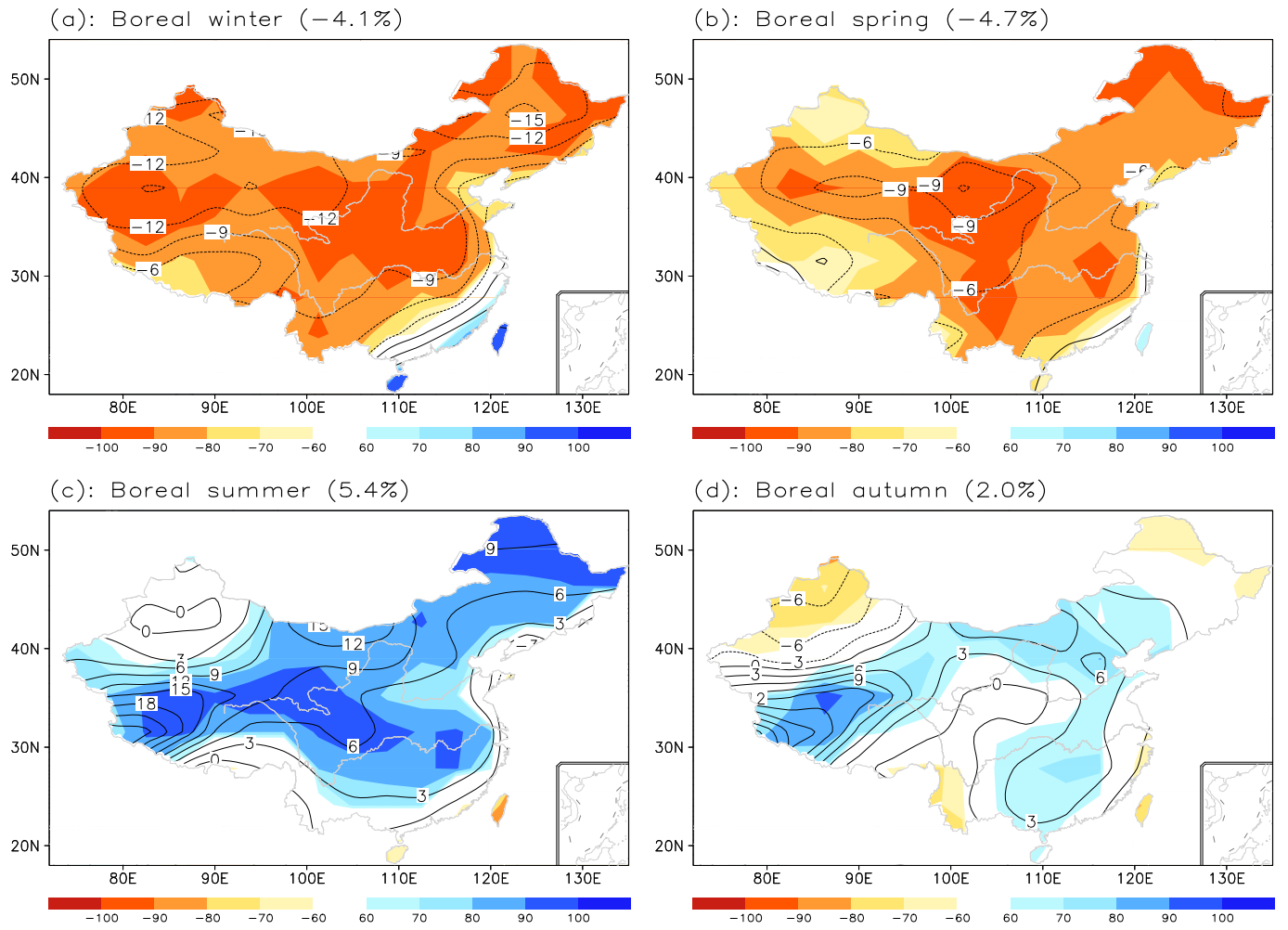

Fig. 8. Percentage changes in seasonal evaporation (contour, units: %) during the mid-Holocene, with reference to the baseline period, for the ensemble mean of the 36 PMIP models. In each panel, the consistency index of the models (units: %) in simulating the direction of the changes in seasonal evaporation is shown in shading, and regionally averaged change in China is given in parentheses.

decreased in most parts of the country, while the opposite held true for summer and autumn on the large scale.

4. Model–data comparison

Given that most proxy data are analyzed and expressed at individual sites and that there has not been a comprehensive overview of available reconstruction records over the whole country in the literature, we collected proxy data site by site. Afterward, two preconditions were arbitrarily set to choose relatively reliable records of the mid-Holocene climate. First, the records had to be published in peer-reviewed journals, which guaranteed the corresponding proxy data and analysis method having been critically reviewed and accepted by the experts in the field of reconstruction; and second, the records had to draw a clear conclusion about the mid-Holocene precipitation and/or moisture conditions over China. In this way, the records of ice cores, lake cores, palaeosols, peat, pollen, sediments, and stalagmites at 74 sites were finally chosen for model–data comparison. For details and references of the records, please refer to Table 2.

There are 13 records of lake cores, peat, pollen, sediments, and stalagmite for precipitation over China (Table 2), all of which indicate that the mid-Holocene precipitation was more than the present level (Fig. 12a). This result is consistent with the proxy data published before the beginning of the 1990s, in which precipitation was estimated to be tens to hundreds of millimeters more than at present in northern China and Tibet, leading to high lake levels, the freshening of inland lakes, the development of large lakes and swamps in North and Northeast China, and the appearance of multi-layered palaeosols in the eolian sand and loess areas (Shi et al., 1993). On the one hand, the MME-PMIP results of annual precipitation (Fig. 2a) agree qualitatively with the records of the lake core, pollen, and sediment at Hulun lake (Wen et al., 2010), the pollen and sediment at Tongjiang (Yang and Wang, 2003), the pollen at Bayanchagan lake (Guiot et al., 2008; Jiang et al., 2010), the pollen and sediment at Diaojiao lake (Shi and Song, 2003), the pollen and lake core at Daihai lake (Xiao et al., 2004; Xu et al., 2010), the pollen at Baiyangdian lake (Xu et al., 1988), the pollen and lake core at Qinghai lake (Kong et al., 1990), the lake core and pollen at Ren Co lake and Hidden lake (Tang et al., 2000), and the peat and pollen at Dahu (Zhou et al., 2004). Quantitatively, however, the models underestimated the reconstructed magnitude of the increase at sites in Northeast and North China, where annual precipitation was

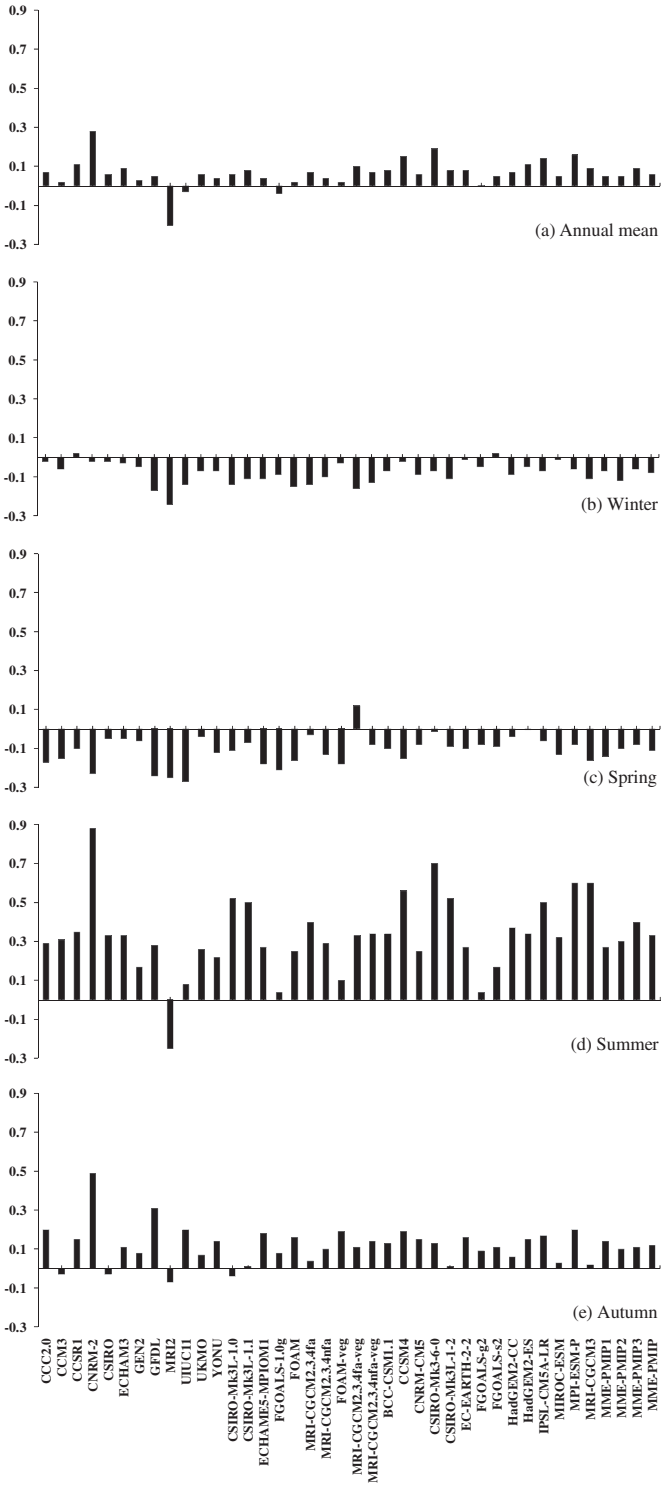

Fig. 9. Changes in regionally averaged annual and seasonal net precipitation (units: mm/day) over China during the mid-Holocene with respect to the baseline period.

estimated to increase by approximately 50 mm at Hulun lake, approximately 150–200 mm at Tongjiang, approximately 30–60% at Bayanchagan lake, approximately 80–200 mm at Diaojiao lake, approximately 40 mm at Daihai lake, and approximately 200 mm at Baiyangdian lake (Table 2). On the other hand, model–data disagreements occurred at Aibi lake (Wu et al., 1996), Heshang Cave (Hu et al., 2008), Mianyang (Yang et al., 1998), and Xinjiang (Shi et al., 1993), where the lesser precipitation simulated by MME-PMIP (Fig. 2a) conflicts with the greater precipitation suggested by the proxy data (Table 2 and Fig. 12a). Note that compared with the present day, the mid-Holocene annual precipitation was also reconstructed to be higher across most parts of China using pollen and/or plant macrofossil data (Bartlein et al., 2011), while it was reconstructed to be generally higher in southern China south of approximately 35°N and Northeast China, but lower or similar to today in Northwest and North China, by applying an inverse modeling technique to pollen data (Guiot et al., 2008), implying a degree of uncertainty in precipitation reconstruction for the latter two regions.

Unlike the extremely sparse distribution of the precipitation reconstructions, most of the collected proxy data provide information of the mid-Holocene moisture conditions. There are records of ice cores, lake cores, palaeosols, peat, pollen, sediments, and stalagmites at 69 sites across China (Table 2). As shown in Fig. 12b, 64 of the 69 records indicate that the mid-Holocene climate was wetter than the present level over the country. On the large scale, a qualitative comparison clearly shows that the aforementioned drier climates derived from the MME-PMIP annual net precipitation changes (Fig. 10a) are of opposite sign to the wetter conditions suggested by the proxy data in Xinjiang and the areas between the middle and lower reaches of the Yangtze and Yellow River valleys. Meanwhile, model–data agreements are registered in the rest of the country, except northern Northeast China where proxy data are not yet available. It should be stressed that although a quality control of the models is performed in Section 2.2, the 36 models chosen for analysis still cannot perfectly reproduce the precipitation climatology over China for the baseline period; and the models differ from one another in the mid-Holocene annual net precipitation changes on the national and regional scales (see Section 3.3), although the model agreements are more than 60% in most parts of China, such as North and South China, the areas between the middle reaches of the Yangtze and Yellow River valleys, Tibet, and southern China (Fig. 10a). Considering there is a large variability in topography and regional climate over East Asia, the smoothed representation of topography is unrealistic in the current coarse-resolution models and hence hampers their accuracy over China (Jiang et al., 2005; Gao et al., 2006); and also there are processes operating in the real world that are fully or mostly missing from the current models, such as carbon and nitrogen dynamics (e.g., Cao and Woodward, 1998; Thornton et al., 2007) and permafrost (e.g., Wania et al., 2009) and soil (e.g., Kutzbach et al., 1996) components in the climate system. Accordingly, there is a level of uncertainty in the climate simulations. Besides, another source of uncertainty lies in the proxy data. It can be observed in Table 2 that in western Inner Mongolia, drier climates were reconstructed at the Juyanze, Zhuyeze, and Toudaohu lakes (Chen et al., 2003), but wetter climates were reconstructed at the adjacent sites of the Badain Jaran desert (Yang et al., 2010), Juyan lake (Chen et al., 2008), Qingtu lake (Long et al., 2010), Yiema lake (Chen et al., 1999), and Zhuyeze lake (Long et al., 2012). Particularly, both drier and wetter conditions were derived from the lake core records at Zhuyeze lake (Chen et al., 2003; Long et al., 2012). In addition, drier climates at Moon lake (Liu et al., 2010b) conflicted with wetter climates at Hulun lake (Yang et al., 1995), and normal

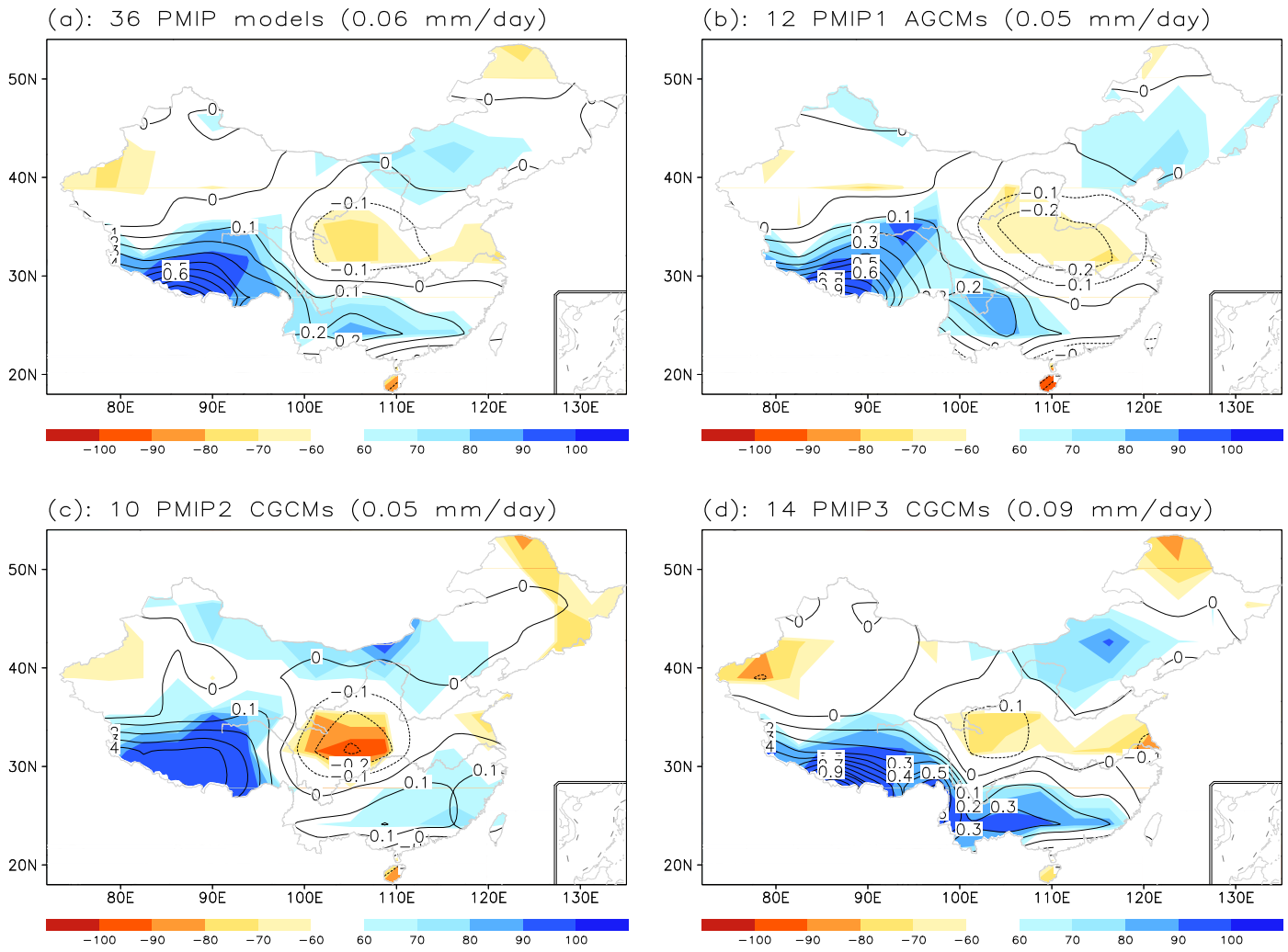

Fig. 10. Mid-Holocene–baseline anomalies of annual net precipitation (contour, units: mm/day) for the ensemble mean of the (a) 36 PMIP models, (b) 12 PMIP1 AGCMs, (c) 10 PMIP2 CGCMs, and (d) 14 PMIP3 CGCMs. In each panel, the consistency index of the models (units: %) in simulating the direction of the changes in annual net precipitation is shown in shading, and regionally averaged change in China is given in parentheses.

conditions at Poyang lake (Ma et al., 2004) disagreed qualitatively with wetter climates at Mianyang (Yang et al., 1998) and at other surrounding sites. Because logically there is only one truth, these disagreements between records emphasize that the proxy data and method used for climatic reconstruction need to be carefully evaluated and validated.

5. Conclusion

In this study, the mid-Holocene annual and seasonal precipitation, evaporation, and net precipitation changes over China were first examined using the results of the PMIP experiments undertaken by 36 reliable climate models, and they were then compared with available proxy data of precipitation and moisture conditions. The primary conclusions are as follows.

(1) The mid-Holocene annual precipitation (evaporation) averaged over China increased in 31 (23) of the 36 PMIP models and by an average of 3.0% (0.9%) compared with the baseline period. Regionally averaged precipitation (evaporation) decreased by 9.9% (4.1%) in winter and by 6.7% (4.7%) in spring but increased by 10.5% (5.4%) in summer and by 6.9% (2.0%) in autumn. The spatial patterns of the changes in annual and seasonal precipitation and evaporation were similar on the large scale.

(2) The mid-Holocene annual net precipitation over China increased in 33 of the 36 PMIP models and by an average of 6.9% or 0.06 mm/day compared with the baseline period. Regionally, the annual net precipitation decreased in Xinjiang but increased in the rest of western China, while it decreased in northern Northeast China and the middle and lower reaches of the Yangtze and Yellow River valleys but increased in the rest of eastern China. Seasonally, net precipitation change was qualitatively consistent among the models, with an average change of −10.0% in winter, −10.1% in spring, 18.6% in summer, and 20.4% in autumn over the country.

(3) A comparison of atmospheric and coupled model simulations indicated that the interactive ocean effect had little impact overall on annual and seasonal precipitation, evaporation (except in autumn), and net precipitation over China during the mid-Holocene.

(4) Based on the records of precipitation at 13 sites and of moisture conditions at 69 sites, both annual precipitation

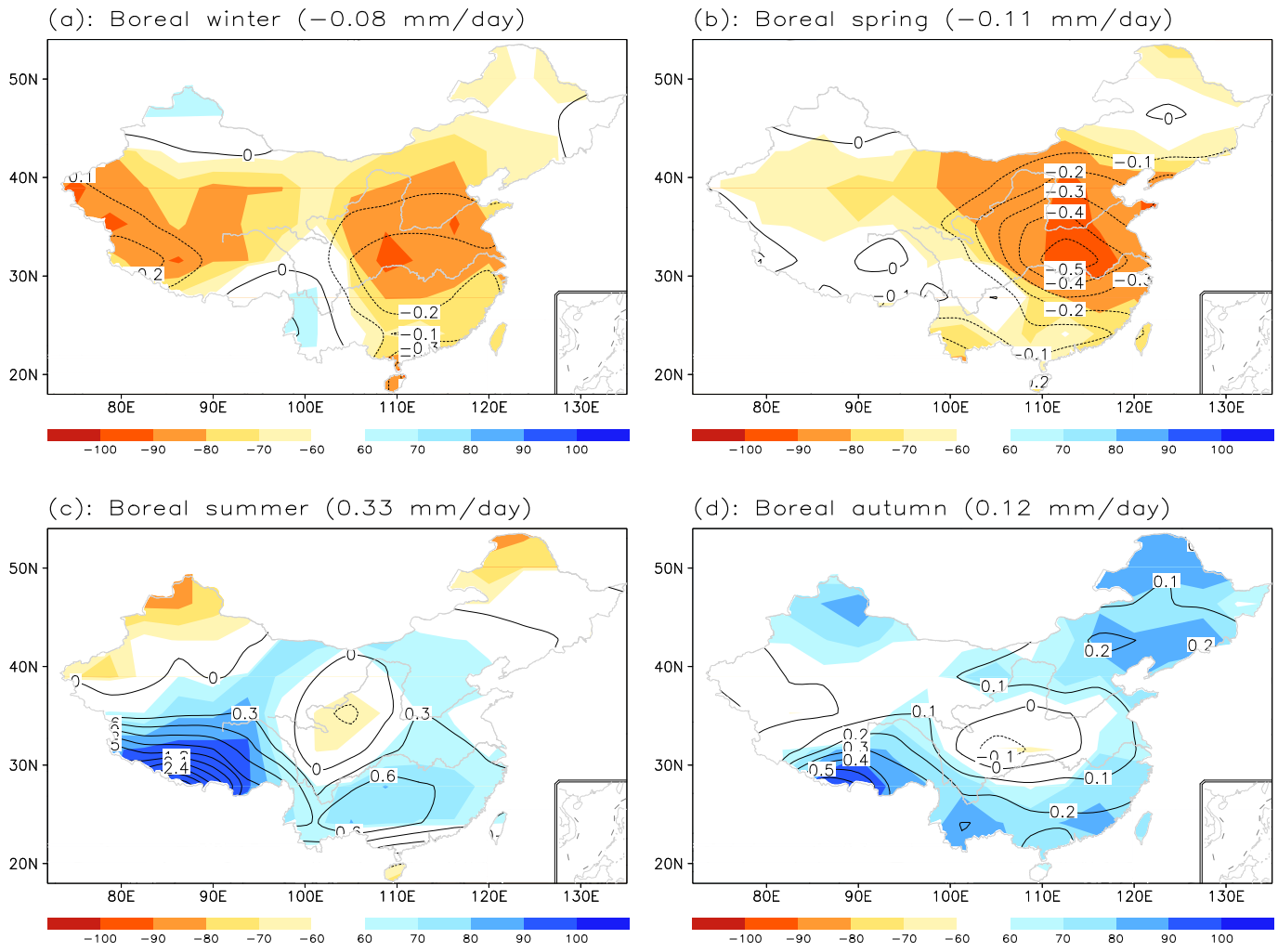

Fig. 11. Mid-Holocene–baseline anomalies of seasonal net precipitation (contour, units: mm/day) for the ensemble mean of the 36 PMIP models. In each panel, the consistency index of the models (units: %) in simulating the direction of the changes in seasonal net precipitation is shown in shading, and regionally averaged change in China is given in parentheses.

Table 2
Proxy data providing estimates of the changes in annual precipitation (ΔP) and/or net precipitation ($\Delta P - \Delta E$) between the mid-Holocene and the present day over China. Data types: 1, lake core; 2, pollen; 3, sediment; 4, palaeosol; 5, peat; 6, stalagmite; 7, ice core.

Site ID		Data type	Latitude (°N)	Longitude (°E)	Elevation (m ASL)	Interval (ka)	$\Delta P - \Delta E$	ΔP	Reference
01	Aibi lake	1, 2, 3	44.88	82.88	194	10.2	Wetter	~26% more	Wu et al. (1996)
02	Angulinao lake	1, 3	41.35	114.39	1310	8.4	Wetter		Zhai et al. (2000)
03	Baahar Nuur lake	1, 3	39.10	109.20	1450	13.9	Wetter		Feng et al. (2005)
04	Badain Jaran desert	3, 5	39.00–40.00	101.00–103.00	1000–1500	10.0	Wetter		Yang et al. (2010)
05	Baimapo	4	34.17	109.32	650	20.6	Wetter		Zhou et al. (1994)
06	Baiyangdian lake	2	38.85	116.00	7	11.0	Wetter	~200 mm more	Xu et al. (1988)
07	Balikun lake	2, 1	43.62	92.77	1575	16.7	Wetter		Tao et al. (2010)
08	Bangong Co lake	1, 2	33.67	79.00	4241	10.0	Wetter		Gasse et al. (1996)
09	Barkol lake	1, 3	43.70	92.83	1580	9.4	Wetter		Xue and Zhong (2008)
10	Baxie	4	35.58	103.57	2000	12.3	Wetter		Zhou et al. (1994)
11	Bayanchagan lake	2	41.65	115.21	1355	12.5	Wetter	More	Guiot et al. (2008)
11	Bayanchagan lake	2	41.65	115.21	1355	12.5	Wetter	~30–60% more	Jiang et al. (2010)
12	Beizhuangcun	4	34.50	109.50	950	26.1	Wetter		Zhou et al. (1994)
13	Bosten lake	1, 3, 2	42.08	87.05	1500	12.0	Wetter		Zhong and Shu (2001)
14	Bosten lake	1, 3	41.95	86.78	1048	8.5	Wetter		Mischke and Wünnemann (2006)
15	Central Inner Mongolia	4, 2, 3	38.61–40.30	109.95–110.41	1037–1312	11.5	Wetter		Sun et al. (2006)
16	Changbaishan	5	40.67–44.50	125.33–131.33	500–900	10.0	Wetter		Zhao et al. (2002)

Table 2 (*continued*)

Site ID		Data type	Latitude (°N)	Longitude (°E)	Elevation (m ASL)	Interval (ka)	$\Delta P-\Delta E$	ΔP	Reference
17	Cuoe lake	2, 3	31.47	91.51	4532	10.5	Wetter		Wu et al. (2006)
18	Dadiwan	2, 3	35.01	105.91	1400	11.2	Wetter		An et al. (2003)
19	Dagushan	2, 3	39.92	123.66	5	8.0–2.5	Wetter		Laboratory of Quaternary palynology and laboratory of radiocarbon, Kweiyang Institute of Geochemistry, Academia Sinica (1978)
20	Dahu	5, 2	24.25	115.03	250	18.0	Wetter	~200 mm more	Zhou et al. (2004)
21	Dahu	2, 5	24.68	115.00	255	18.3	Wetter		Xiao et al. (2007)
22	Daihai lake	2	40.58	112.69	1221	12.0	Wetter	~40 mm more	Xu et al. (2010)
22	Daihai lake	2, 1	40.58	112.69	1221	10.2	Wetter	More	Xiao et al. (2004)
23	Daziying	2, 5	39.70	118.99	5	9.8	Wetter		Li and Liang (1985)
24	Diaojiao lake	2, 3	41.30	112.35	1800	10.1	Wetter		Song et al. (1996)
24	Diaojiao lake	2, 3	41.30	112.35	1800	10.1	Wetter	~80–200 mm more	Shi and Song (2003)
25	Dingxi	4	35.52	104.54	1950	8.9	Wetter		Feng et al. (2005)
26	Dongganchi	2	39.53	115.78	49	15.8	Wetter		Zhang and Kong (1999)
27	Dongge cave	6	25.28	108.08	680	15.4	Wetter		Zhang et al. (2004)
28	Erhai lake	1, 2, 3	25.78	100.19	1974	10.8	Wetter		Zhou et al. (2003)
29	Gonong Co	2, 3	34.63	92.15	4670	19.2	Wetter		Li et al. (1995)
30	Guliya	7	35.28	81.48	6200	125.0	Wetter		Thompson et al. (1997)
31	Gushantun bog	3	42.00	126.00	500	13.5	Wetter		Wang and Liu (2001)
32	Ha'ni	1, 2, 3	42.23	126.52	900	13.1–4.5	Wetter		Yu et al. (2008)
33	Haoluku lake	3, 2	42.96	116.76	1295	10.2	Wetter		Wang et al. (2001)
34	Heshang cave	6	30.45	110.42	294	9.4		8% more	Hu et al. (2008)
35	Hidden lake	1, 2	29.81	92.54	4980	14.0		~200 mm more	Tang et al. (2000)
36	Huguangyan Maar lake	1, 2	21.15	110.28	23	13.0	Wetter		Wang et al. (2007)
37	Hulu river	3, 2	35.00	106.00	1540	8.0–3.0	Wetter		Mo et al. (1996)
38	Hulun lake	2, 3	48.90	116.50	544	19.9	Wetter		Yang et al. (1995)
39	Hulun lake	1, 2, 3	49.13	117.51	545	11.0		~50 mm more	Wen et al. (2010)
40	Jingbo lake	1, 2	43.90	128.80	350	9.6	Wetter		Li et al. (2011a)
41	Juyan lake	2	41.80	101.80	892	10.7	Wetter		Chen et al. (2008)
42	Juyanze lake	1, 3, 2	41.89	101.85	892	9.4	Drier		Chen et al. (2003)
43	Kouka lake	1, 3	34.01	97.24	4530	16.3	Wetter		Mischke et al. (2008)
44	Longzhong basin	2, 4	35.00–35.55	104.52–105.91	1400–1889	12.2	Wetter		Tang and An (2007)
45	Manas lake	1, 3, 2	45.75	86.00	251	37.0	Wetter		Rhodes et al. (1996)
46	Maohebei	2, 5	39.50	119.17	50	10.3	Wetter		Li and Liang (1985)
47	Mianyang	2	30.20	113.22	24	10.0	Wetter	More	Yang et al. (1998)
48	Moon lake	1, 3, 2	47.51	120.87	1190	21.0	Drier		Liu et al. (2010b)
49	Naleng lake	2, 1	31.10	99.75	4200	11.7	Wetter		Cramer et al. (2010)
50	Nam Co lake	1, 3	30.84	90.90	4718	8.4	Wetter		Lin et al. (2008)
50	Nam Co lake	2, 1	30.84	90.90	4718	8.4	Wetter		Li et al. (2011b)
51	Otindag	4, 3	41.41–43.69	114.97–117.66	1200–1400	9.9	Wetter		Zhou et al. (2008)
52	Poyang lake	1, 3	29.03	116.14	8	7.9	Normal		Ma et al. (2004)
53	Qinghai lake	2, 1	36.55	99.60	3196	11.0		At least 100 mm more	Kong et al. (1990)
54	Qingtu lake	3	39.05	103.67	1309	9.5–2.5	Wetter		Long et al. (2010)
55	Ren Co lake	1, 2	30.73	96.68	4450	18.0		~200 mm more	Tang et al. (2000)
56	Renjiahutong	4	35.75	109.42	1100	13.0	Wetter		Zhou et al. (1994)
57	Rutog	3, 2	33.39	79.73	4265	6.5	Wetter		Wang et al. (2010b)
58	Shanbao cave	6	31.67	110.43	1902	11.5–2.1	Wetter		Shao et al. (2006)
59	Siling Co lake	1, 3	31.60	89.05	4530	12.8	Wetter		Kashiwaya et al. (1995)
60	Sujiawan	2, 3	35.54	104.52	1700	8.9	Wetter		An et al. (2003)
61	Sumxi Co lake	1, 3	34.62	81.03	5058	13.0	Wetter		Gasse et al. (1991)
62	Tanghongling	2, 3	48.35	129.67	465	9.0	Wetter		Yang and Wang (2002)
63	Tongjiang	2, 3	48.08	133.25	60	8.0	Wetter	150–200 mm more	Yang and Wang (2003)
64	Toudaohu lake	1, 3, 2	38.42	105.12	1351	6.3	Drier		Chen et al. (2003)
65	Ulungur lake	1, 3	47.22	87.15	478	9.9	Wetter		Jiang et al. (2007)
66	Wutonggou	3	44.39	87.86	429	18.3	Wetter		Li and Fan (2011)
67	Xiangshui cave	6	25.25	110.92	400	6.0	Wetter		Zhang et al. (2003)
68	Xianrendong cave	6	25.83	103.50	1810	8.0	Wetter		Zhang et al. (2009)
69	Yiema lake	1, 3	39.10	103.67	1312	16.0	Wetter		Chen et al. (1999)
70	Zhuyeze lake	1, 3, 2	39.01	103.34	1320	15.2	Drier		Chen et al. (2003)
71	Zhuyeze lake	1	39.17	104.16	1291	80	Wetter		Long et al. (2012)
72	Zigê Tangco	1, 3	32.08	90.84	4560	10.5	Wetter		Wu et al. (2007)
73	Zigetang lake	1, 2	32.00	90.90	4560	10.8	Wetter		Herzschuh et al. (2006)
74	Zoige	2	33.90	102.55	3396	20.0	Wetter		Liu et al. (1995)

and net precipitation were generally higher than the present level over China during the mid-Holocene. Qualitatively, the models disagreed with the multi-proxy data in Xinjiang and the areas between the middle and lower reaches of the Yangtze and Yellow River valleys where drier-than-baseline climates were obtained from the 36 models, while model–data agreements were presented in the rest of the country. There are uncertainties in both the model simulations and in the proxy data, as discussed in Section 4, which require further studies.

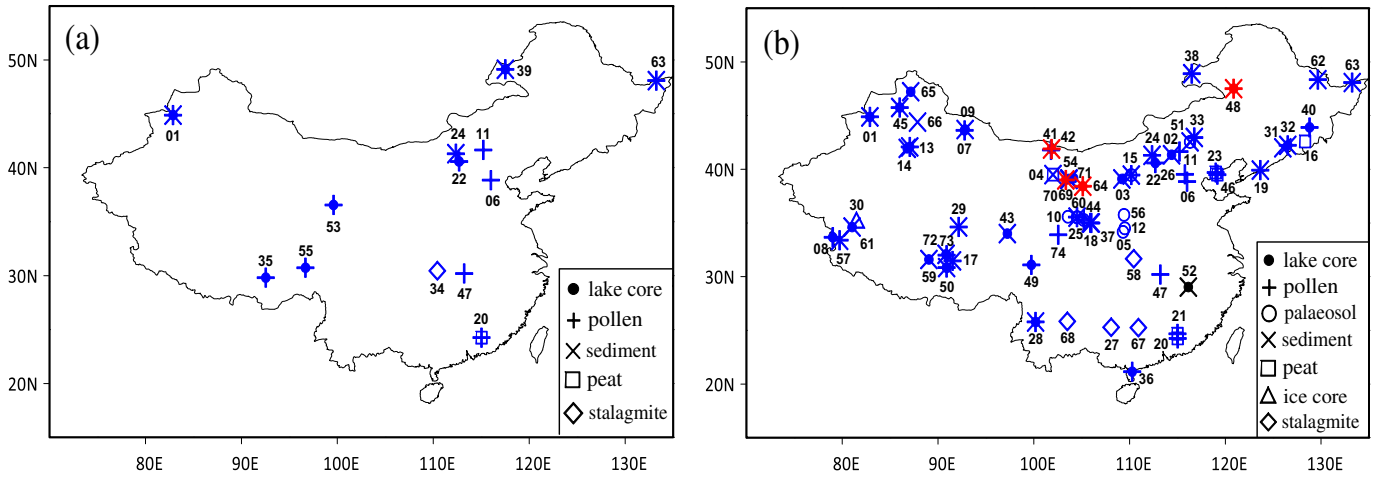

Fig. 12. Proxy estimates of the changes in annual (a) precipitation at 13 sites and (b) net precipitation at 69 sites during the mid-Holocene relative to the present period, in which blue, black, and red symbols represent wetter, normal, and drier conditions, respectively, and number represents site ID (see Table 2 for details and references). (For interpretation of the references to color in this figure legend, the reader is referred to the web version of this article.)

Acknowledgments

We sincerely thank the two anonymous reviewers and the editor for their helpful comments on the manuscript and thank Fahu Chen, Zhongping Lai, Shenghua Li, Huayu Lu, Jimin Sun, Hailei Wang, and Hongya Wang for providing information on proxy data. Also, we acknowledge the international modeling groups for providing their data for analysis, the Laboratoire des Sciences du Climat et de l'Environnement (LSCE) for collecting and archiving the model data. This work was supported by the Strategic Priority Research Program (XDA05120703 and XDB03020602) and the Knowledge Innovation Program (KZCX2-EW-QN202) of the Chinese Academy of Sciences and by the National Natural Science Foundation of China (41222034 and 41175072). The PMIP2/MOTIF Data Archive is supported by CEA, CNRS, the EU project MOTIF (EVK2-CT-2002-00153) and the Programme National d'Etude de la Dynamique du Climat (PNEDC). The analyses were performed using version 30 November 2012 of the database. More information is available on http://pmip3.lsce.ipsl.fr/, http://pmip2.lsce.ipsl.fr/, and http://motif.lsce.ipsl.fr/.

References

An, C., Feng, Z., Tang, L., 2003. Evidence of a humid mid-Holocene in the western part of Chinese Loess Plateau. Chin. Sci. Bull. 48, 2472–2479.
Bartlein, P.J., Harrison, S.P., Brewer, S., Connor, S., Davis, B.A.S., Gajewski, K., Guiot, J., Harrison-Prentice, T.I., Henderson, A., Peyron, O., Prentice, I.C., Scholze, M., Seppä, H., Shuman, B., Sugita, S., Thompson, R.S., Viau, A.E., Williams, J., Wu, H., 2011. Pollen-based continental climate reconstructions at 6 and 21 ka: a global synthesis. Clim. Dyn. 37, 775–802.
Berger, A., 1978. Long-term variations of daily insolation and Quaternary climatic changes. J. Atmos. Sci. 35, 2362–2367.
Braconnot, P., Otto-Bliesner, B., Harrison, S., Joussaume, S., Peterchmitt, J.-Y., Abe-Ouchi, A., Crucifix, M., Driesschaert, E., Fichefet, Th., Hewitt, C.D., Kageyama, M., Kitoh, A., Laîné, A., Loutre, M.-F., Marti, O., Merkel, U., Ramstein, G., Valdes, P., Weber, S.L., Yu, Y., Zhao, Y., 2007. Results of PMIP2 coupled simulations of the mid-Holocene and last glacial maximum – part 1: experiments and large-scale features. Clim. Past 3, 261–277.
Cao, M., Woodward, F.I., 1998. Dynamic responses of terrestrial ecosystem carbon cycling to global climate change. Nature 393, 249–252.
Chen, F., Shi, Q., Wang, J., 1999. Environmental changes documented by sedimentation of Lake Yiema in arid China since the late glaciation. J. Paleolimnol. 22, 159–169.
Chen, F., Wu, W., Holmes, J.A., Madsen, D.B., Zhu, Y., Jin, M., Oviatt, C.G., 2003. A mid-Holocene drought interval as evidenced by lake desiccation in the Alashan Plateau, Inner Mongolia, China. Chin. Sci. Bull. 48, 1401–1410.
Chen, F., Yu, Z., Yang, M., Ito, E., Wang, S., Madsen, D.B., Huang, X., Zhao, Y., Sato, T., Birks, H.J.B., Boomer, I., Chen, J., An, C., Wünnemann, B., 2008. Holocene moisture evolution in arid central Asia and its out-of-phase relationship with Asian monsoon history. Quat. Sci. Rev. 27, 351–364.
Chen, X., Yu, G., Liu, J., 2002. Mid-Holocene climate simulation and discussion on the mechanism of temperature changes in eastern Asia. Sci. China Earth Sci. 32, 335–345 (in Chinese).
Cramer, A., Herzschuh, U., Mischke, S., Zhang, C., 2010. Holocene treeline shifts and monsoon variability in the Hengduan Mountains (southeastern Tibetan Plateau), implications from palynological investigations. Palaeogeogr. Palaeoclimatol. Palaeoecol. 286, 23–41.
Dallmeyer, A., Claussen, M., Otto, J., 2010. Contribution of oceanic and vegetation feedbacks to Holocene climate change in monsoonal Asia. Clim. Past 6, 195–218.
Feng, Z.D., Wang, W.G., Guo, L.L., Khosbayar, P., Narantsetseg, T., Jull, A.J.T., An, C.B., Li, X.Q., Zhang, H.C., Ma, Y.Z., 2005. Lacustrine and eolian records of Holocene climate changes in the Mongolian Plateau: preliminary results. Quat. Int. 136, 25–32.
Ganopolski, A., Kubatzki, C., Claussen, M., Brovkin, V., Petoukhov, V., 1998. The influence of vegetation–atmosphere–ocean interaction on climate during the mid-Holocene. Science 280, 1916–1919.
Gao, X., Xu, Y., Zhao, Z., Pal, J.S., Giorgi, F., 2006. On the role of resolution and topography in the simulation of East Asia precipitation. Theor. Appl. Climatol. 86, 173–185.
Gasse, F., Arnold, M., Fontes, J.C., Fort, M., Gibert, E., Huc, A., Li, B., Li, Y., Liu, Q., Mélières, F., Van Campo, E., Wang, F., Zhang, Q., 1991. A 13,000-year climate record from western Tibet. Nature 353, 742–745.
Gasse, F., Fontes, J.C., Van Campo, E., Wei, K., 1996. Holocene environmental changes in Bangong Co basin (Western Tibet). Part 4: discussion and conclusions. Palaeogeogr. Palaeoclimatol. Palaeoecol. 120, 79–92.
Guiot, J., Boreux, J.J., Braconnot, P., Torre, F., PMIP Participants, 1999. Data–model comparison using fuzzy logic in paleoclimatology. Clim. Dyn. 15, 569–581.
Guiot, J., Wu, H.B., Jiang, W.Y., Luo, Y.L., 2008. East Asian monsoon and paleoclimatic data analysis: a vegetation point of view. Clim. Past 4, 137–145.
Herzschuh, U., Winter, K., Wünnemann, B., Li, S., 2006. A general cooling trend on the central Tibetan Plateau throughout the Holocene recorded by the Lake Zigetang pollen spectra. Quat. Int. 154–155, 113–121.
Hu, C., Henderson, G.M., Huang, J., Xie, S., Sun, Y., Johnson, K.R., 2008. Quantification of Holocene Asian monsoon rainfall from spatially separated cave records. Earth Planet. Sci. Lett. 266, 221–232.
Jansen, E., Overpeck, J., Briffa, K.R., Duplessy, J.-C., Joos, F., Masson-Delmotte, V., Olago, D., Otto-Bliesner, B., Peltier, W.R., Rahmstorf, S., Ramesh, R., Raynaud, D., Rind, D., Solomina, O., Villalba, R., Zhang, D., 2007. Palaeoclimate. In: Solomon, S., Qin, D., Manning, M., Chen, Z., Marquis, M., Averyt, K.B., Tignor, M., Miller, H.L. (Eds.), Climate Change 2007: the Physical Science Basis. Contribution of Working Group I to the Fourth Assessment Report of the Intergovernmental Panel on Climate Change. Cambridge University Press, Cambridge, United Kingdom and New York, NY, USA, pp. 434–497.
Jiang, D., Wang, H.J., Lang, X., 2005. Evaluation of East Asian climatology as simulated by seven coupled models. Adv. Atmos. Sci. 22, 479–495.
Jiang, D., Lang, X., Tian, Z., Wang, T., 2012. Considerable model–data mismatch in temperature over China during the mid-Holocene: results of PMIP simulations. J. Clim. 25, 4135–4153.
Jiang, D., Lang, X., Tian, Z., Ju, L., 2013. Mid-Holocene East Asian summer monsoon strengthening: insights from Paleoclimate Modeling Intercomparison Project (PMIP) simulations. Palaeogeogr. Palaeoclimatol. Palaeoecol. 369, 422–429.
Jiang, Q.F., Shen, J., Liu, X.Q., Zhang, E.L., 2007. Holocene climate reconstruction of Ulungur Lake (Xinjiang, China) inferred from ostracod species assemblages and stable isotopes. Quat. Sci. 27, 382–391 (in Chinese).

Jiang, W., Guiot, J., Chu, G., Wu, H., Yuan, B., Hatté, C., Guo, Z., 2010. An improved methodology of the modern analogues technique for palaeoclimate reconstruction in arid and semi-arid regions. Boreas 39, 145–153.
Joussaume, S., Taylor, K.E., 1995. Status of the paleoclimate modeling Intercomparison project (PMIP). In: Gates, W.L. (Ed.), Proceedings of the First International AMIP Scientific Conference, WCRP-92, WMO/TD-732. World Meteorological Organization, Geneva, pp. 425–430.
Kashiwaya, K., Masuzawa, T., Morinaga, H., Yaskawa, K., Yuan, B., Liu, J., Gu, Z., 1995. Changes in hydrological conditions in the central Qing-Zang (Tibetan) Plateau inferred from lake bottom sediments. Earth Planet. Sci. Lett. 135, 31–39.
Kong, Z.C., Du, N.Q., Shan, F.S., Tong, G.B., Luo, S.J., Fan, S.X., 1990. Vegetational and climatic changes in the last 11,000 years in Qinghai Lake — numerical analysis based on palynology in core QH85-14C. Mar. Geology. Quat. Geology. 10, 79–90 (in Chinese).
Kutzbach, J., Bonan, G., Foley, J., Harrison, S.P., 1996. Vegetation and soil feedbacks on the response of the African monsoon to orbital forcing in the early to middle Holocene. Nature 384, 623–626.
Laboratory of Quaternary palynology and laboratory of radiocarbon, Kweiyang Institute of Geochemistry, Academia Sinica, 1978. Development of natural environment in the southern part of Liaoning Province during the last 10,000 years. Sci. China Math. 21, 516–532.
Li, B.Y., Li, Y.F., Kong, Z.C., Shan, F.S., Zhu, L.P., Li, S.K., 1995. 20,000 years environmental changes of the Gonong Co in Hoh Xil of Qinghai. Chin. Sci. Bull. 40, 1055–1056.
Li, C.H., Wu, Y.H., Hou, X.H., 2011a. Holocene vegetation and climate in Northeast China revealed from Jingbo Lake sediment. Quat. Int. 229, 67–73.
Li, Q., Lu, H., Zhu, L., Wu, N., Wang, J., Lu, X., 2011b. Pollen-inferred climate changes and vertical shifts of alpine vegetation belts on the northern slope of the Nyainqentanglha Mountains (central Tibetan Plateau) since 8.4 kyr BP. Holocene 21, 939–950.
Li, S., Fan, A., 2011. OSL chronology of sand deposits and climate change of last 18 ka in Gurbantunggut Desert, northwest China. J. Quat. Sci. 26, 813–818.
Li, W.Y., Liang, Y.L., 1985. Vegetation and environment of the Hypsithermal Interval of Holocene in eastern Hebei Plain. Acta Bot. Sin. 27, 640–651 (in Chinese).
Lin, X., Zhu, L., Wang, Y., Wang, J., Xie, M., Ju, J., Mäusbacher, R., Schwalb, A., 2008. Environmental changes reflected by n-alkanes of lake core in Nam Co on the Tibetan Plateau since 8.4 ka B.P. Chin. Sci. Bull. 53, 3051–3057.
Liu, G.X., Shen, Y.P., Wang, R., Wang, S.M., 1995. The vegetation and climatic changes in Zoige during the last 20000 years determined by pollen records. J. Glaciol. Geocryol. 17, 132–137 (in Chinese).
Liu, Q., Li, Q., Wang, L., Chu, G.Q., 2010b. Stable carbon isotope record of bulk organic matter from a sediment core at Moon Lake in the middle part of the Daxing'an Mountain range, Northeast China during the last 21 ka. Quat. Sci. 30, 1069–1077 (in Chinese).
Liu, Y., He, J., Li, W., Chen, L., Li, W., Zhang, B., 2010a. MM5 simulations of the China regional climate during the mid-Holocene. Acta Meteorol. Sin 24, 468–483.
Liu, Z., Harrison, S.P., Kutzbach, J., Otto-Bliesner, B., 2004. Global monsoons in the mid-Holocene and oceanic feedback. Clim. Dyn. 22, 157–182.
Long, H., Lai, Z., Wang, N., Li, Y., 2010. Holocene climate variations from Zhuyeze terminal lake records in East Asian monsoon margin in arid northern China. Quat. Res. 74, 46–56.
Long, H., Lai, Z., Fuchs, M., Zhang, J., Li, Y., 2012. Timing of Late Quaternary palaeolake evolution in Tengger Desert of northern China and its possible forcing mechanisms. Glob. Planet. Change 92–93, 119–129.
Ma, Z.X., Huang, J.H., Wei, Y., Li, J.H., Hu, C.Y., 2004. Organic carbon isotope records of the Poyang Lake sediments and their implications for the paleoclimate during the last 8 ka. Geochimica 33, 279–285 (in Chinese).
Marzin, C., Braconnot, P., 2009. The role of the ocean feedback on Asian and African monsoon variations at 6 kyr and 9.5 kyr BP. C. R. Geosci. 341, 643–655.
Masson-Delmotte, V., Kageyama, M., Braconnot, P., Charbit, S., Krinner, G., Ritz, C., Guilyardi, E., Jouzel, J., Abe-Ouchi, A., Crucifix, M., Gladstone, R.M., Hewitt, C.D., Kitoh, A., LeGrande, A.N., Marti, O., Merkel, U., Motoi, T., Ohgaito, R., Otto-Bliesner, B., Peltier, W.R., Ross, I., Valdes, P.J., Vettoretti, G., Weber, S.L., Wolk, F., Yu, Y., 2006. Past and future polar amplification of climate change: climate model intercomparisons and ice-core constraints. Clim. Dyn. 26, 513–529.
Mischke, S., Wünnemann, B., 2006. The Holocene salinity history of Bosten Lake (Xinjiang, China) inferred from ostracod species assemblages and shell chemistry: possible palaeoclimatic implications. Quat. Int. 154–155, 100–112.
Mischke, S., Kramer, M., Zhang, C., Shang, H., Herzschuh, U., Erzinger, J., 2008. Reduced early Holocene moisture availability in the Bayan Har Mountains, northeastern Tibetan Plateau, inferred from a multi-proxy lake record. Palaeogeogr. Palaeoclimatol. Palaeoecol. 267, 59–76.
Mo, D.W., Li, F., Li, S.C., Kong, Z.C., 1996. A preliminary study of the paleoenvironment of the middle Holocene in the Hulu River area in Gansu Province and its effects on human activity. Acta Geogr. Sin. 51, 59–69 (in Chinese).
Peyron, O., Jolly, D., Braconnot, P., Bonnefille, R., Guiot, J., Wirrmann, D., Chalié, F., 2006. Quantitative reconstructions of annual rainfall in Africa 6000 years ago: model–data comparison. J. Geophys. Res. 111, D24110. http://dx.doi.org/10.1029/2006JD007396.
Rhodes, T.E., Gasse, F., Lin, R.F., Fontes, J., Wei, K.Q., Bertrand, P., Gibert, E., Mélières, F., Tucholka, P., Wang, Z.X., Cheng, Z.Y., 1996. A late Pleistocene–Holocene lacustrine record from Lake Manas, Zunggar (northern Xinjiang, western China). Palaeogeogr. Palaeoclimatol. Palaeoecol. 120, 105–121.
Shao, X., Wang, Y., Cheng, H., Kong, X., Wu, J., Lawrence, E.R., 2006. Long-term trend and abrupt events of the Holocene Asian monsoon inferred from a stalagmite $\delta^{18}O$ record from Shennongjia in central China. Chin. Sci. Bull. 51, 221–228.
Shi, P.J., Song, C.Q., 2003. Palynological records of environmental changes in the middle part of Inner Mongolia, China. Chin. Sci. Bull. 48, 1433–1438.
Shi, Y., Kong, Z., Wang, S., Tang, L., Wang, F., Yao, T., Zhao, X., Zhang, P., Shi, S., 1993. Mid-Holocene climates and environments in China. Glob. Planet. Change 7, 219–233.
Song, C.Q., Wang, B.Y., Sun, X.J., 1996. Implication of paleovegetational changes in Diaojiao Lake, Inner Mongolia. Acta Bot. Sin. 38, 568–575 (in Chinese).
Sui, Y., Jiang, D., Tian, Z., 2013. Latest update of the climatology and changes in the seasonal distribution of precipitation over China. Theor. Appl. Climatol. 113, 599–610.
Sun, J., Li, S., Han, P., Chen, Y., 2006. Holocene environmental changes in the central Inner Mongolia, based on single-aliquot-quartz optical dating and multi-proxy study of dune sands. Palaeogeogr. Palaeoclimatol. Palaeoecol. 233, 51–62.
Tang, L.Y., An, C.B., 2007. Pollen records of Holocene vegetation and climate changes in the Longzhong Basin of the Chinese Loess Plateau. Prog. Nat. Sci. 17, 1445–1456.
Tang, L.Y., Shen, C.M., Liu, K., Overpeck, J.T., 2000. Changes in South Asian monsoon: new high-resolution paleoclimatic records from Tibet, China. Chin. Sci. Bull. 45, 87–91.
Tao, S., An, C., Chen, F., Tang, L., Wang, Z., Lü, Y., Li, Z., Zheng, T., Zhao, J., 2010. Pollen-inferred vegetation and environmental changes since 16.7 ka BP at Balikun Lake, Xinjiang. Chin. Sci. Bull. 55, 2449–2457.
Tarasov, P.E., Guiot, J., Cheddadi, R., Andreev, A.A., Bezusko, L.G., Blyakharchuk, T.A., Dorofeyuk, N.I., Filimonova, L.V., Volkova, V.S., Zernitskaya, V.P., 1999. Climate in northern Eurasia 6000 years ago reconstructed from pollen data. Earth Planet. Sci. Lett. 171, 635–645.
Taylor, K.E., 2001. Summarizing multiple aspects of model performance in a single diagram. J. Geophys. Res. 106 (D7), 7183–7192.
Thompson, L.G., Yao, T., Davis, M.E., Henderson, K.A., Mosley-Thompson, E., Lin, P.-N., Beer, J., Synal, H.-A., Cole-Dai, J., Bolzan, J.F., 1997. Tropical climate instability: the last glacial cycle from a Qinghai–Tibetan ice core. Science 276, 1821–1825.
Thornton, P.E., Lamarque, J.-F., Rosenbloom, N.A., Mahowald, N.M., 2007. Influence of carbon–nitrogen cycle coupling on land model response to CO_2 fertilization and climate variability. Glob. Biogeochem. Cycle 21, GB4018. http://dx.doi.org/10.1029/2006GB002868.
Wang, G., 2005. Agricultural drought in a future climate: results from 15 global climate models participating in the IPCC 4th assessment. Clim. Dyn. 25, 739–753.
Wang, H.J., 1999. Role of vegetation and soil in the Holocene megathermal climate over China. J. Geophys. Res. 104 (D8), 9361–9367.
Wang, H.J., 2000. The seasonal climate and low frequency oscillation in the simulated mid-Holocene megathermal climate. Adv. Atmos. Sci. 17, 445–457.
Wang, H.J., 2002. The mid-Holocene climate simulated by a grid-point AGCM coupled with a biome model. Adv. Atmos. Sci. 19, 205–218.
Wang, H.L., Liu, J.Y., Wang, C.M., 2010b. Paleoenvironment of ostracods and pollen record since middle Holocene in Rutog Area, Tibet. Acta Geol. Sin. 84, 1680–1689 (in Chinese).
Wang, H.Y., Liu, H.Y., Cui, H.T., Abrahamsen, N., 2001. Terminal Pleistocene/Holocene palaeoenvironmental changes revealed by mineral-magnetism measurements of lake sediments for Dali Nor area, southeastern Inner Mongolia Plateau, China. Palaeogeogr. Palaeoclimatol. Palaeoecol. 170, 115–132.
Wang, J.Q., Liu, J.L., 2001. The records of amino acids and organic carbon isotope for Holocene Megathermal in Changbaishan area. Acta Micropalaeontol. Sin. 18, 392–398 (in Chinese).
Wang, L., Chen, W., 2010. How well do existing indices measure the strength of the East Asian winter monsoon? Adv. Atmos. Sci. 27, 855–870.
Wang, S.Y., Lü, H.Y., Liu, J.Q., Negendank, J.F.W., 2007. The early Holocene optimum inferred from a high-resolution pollen record of Huguangyan Maar Lake in southern China. Chin. Sci. Bull. 52, 2829–2836.
Wang, T., Wang, H.J., Jiang, D., 2010a. Mid-Holocene East Asian summer climate as simulated by the PMIP2 models. Palaeogeogr. Palaeoclimatol. Palaeoecol. 288, 93–102.
Wania, R., Ross, I., Prentice, I.C., 2009. Integrating peatlands and permafrost into a dynamic global vegetation model: 2. Evaluation and sensitivity of vegetation and carbon cycle processes. Glob. Biogeochem. Cycle 23, GB3015. http://dx.doi.org/10.1029/2008GB003413.
Wei, J., Wang, H.J., 2004. A possible role of solar radiation and ocean in the mid-Holocene East Asian monsoon climate. Adv. Atmos. Sci. 21, 1–12.
Wen, R.L., Xiao, J.L., Chang, Z.G., Zhai, D.Y., Zhou, L., Xu, Q.H., Li, Y.C., Itoh, S., 2010. Holocene vegetation and climate changes reflected by the pollen record of Hulun Lake, north eastern Inner Mongolia. Quat. Sci. 30, 1105–1115 (in Chinese).
Wu, J.L., Wang, S.M., Wang, H.D., 1996. Characters of the evolution of climate and environment of Holocene in Aibi Lake basin in Xinjiang. Oceanol. Limnol. Sin. 27, 524–530 (in Chinese).
Wu, Y., Lücke, A., Jin, Z., Wang, S., Schleser, G.H., Battarbee, R.W., Xia, W., 2006. Holocene climate development on the central Tibetan Plateau: a sedimentary record from Cuoe Lake. Palaeogeogr. Palaeoclimatol. Palaeoecol. 234, 328–340.
Wu, Y., Lücke, A., Wünnemann, B., Li, S., Wang, S., 2007. Holocene climate change in the central Tibetan Plateau inferred by lacustrine sediment geochemical records. Sci. China Earth Sci. 50, 1548–1555.

Xiao, J.L., Xu, Q.H., Nakamura, T., Yang, X.L., Liang, W.D., Inouchi, Y., 2004. Holocene vegetation variation in the Daihai Lake region of north-central China: a direct indication of the Asian monsoon climatic history. Quat. Sci. Rev. 23, 1669–1679.
Xiao, J.Y., Lü, H.B., Zhou, W.J., Zhao, Z.J., Hao, R.H., 2007. Evolution of vegetation and climate since the last glacial maximum recorded at Dahu peat site, South China. Sci. China Earth Sci. 50, 1209–1217.
Xie, P., Arkin, P.A., 1997. Global precipitation: a 17-year monthly analysis based on gauge observations, satellite estimates, and numerical model outputs. Bull. Amer. Meteorol. Soc. 78, 2539–2558.
Xu, Q., Chen, S., Kong, Z., Du, N., 1988. Preliminary discussion of vegetation succession and climatic change since the Holocene in the Baiyangdian Lake district. Acta Phytoecol. Geobot. Sin. 12, 143–151 (in Chinese).
Xu, Q., Xiao, J., Li, Y., Tian, F., Nakagawa, T., 2010. Pollen-based quantitative reconstruction of Holocene climate changes in the Daihai Lake area, Inner Mongolia, China. J. Clim. 23, 2856–2868.
Xue, J.B., Zhong, W., 2008. Holocene climate change recorded by lacustrine sediments in Barkol Lake and its regional comparison. Quat. Sci. 28, 610–620 (in Chinese).
Yang, X., Ma, N., Dong, J., Zhu, B., Xu, B., Ma, Z., Liu, J., 2010. Recharge to the interdune lakes and Holocene climatic changes in the Badain Jaran Desert, western China. Quat. Res. 73, 10–19.
Yang, X.D., Wang, S.M., Xue, B., Tong, G.B., 1995. Vegetational development and environmental changes in Hulun Lake since late Pleistocene. Acta Palaeontol. Sin. 34, 647–656 (in Chinese).
Yang, X.D., Zhu, Y.X., Jiang, X.Z., Wu, Y.H., Wang, S.M., 1998. Environmental changes from spore-pollen record of Mianyang region over the past 10000 years. J. Lake Sci. 10, 23–29 (in Chinese).
Yang, Y.X., Wang, S.Y., 2002. Study on mire development and palaeoenvironment change since 9.0 ka B.P. in the east part of the Xiaoxinganling Mountains. J. Mountain Sci. 20, 129–134 (in Chinese).
Yang, Y.X., Wang, S.Y., 2003. Study on mire development and paleoenvironment change since 8.0 ka B.P. in the northern part of the Sanjiang Plain. Scientia Geographica Sinica 23, 32–38 (in Chinese).
Yu, C.X., Luo, Y.L., Sun, X.J., 2008. A high-resolution pollen records from Ha'ni Lake, Jilin, Northeast China showing climate changes between 13.1 cal. ka B.P. and 4.5 cal. ka B.P. Quat. Sci. 28, 929–938 (in Chinese).
Zhai, Q.M., Qiu, W.L., Li, R.Q., Zhao, Y., Zheng, L.M., 2000. The middle and late Holocene lacustrine sediments and its climate significance of Angulinao–Bojianghaizi Lakes, Inner Mongolia. J. Palaeogeogr. 2, 84–91 (in Chinese).
Zhang, H.L., Qin, J.M., Lin, Y.S., Pu, X.Q., Liu, C.H., 2009. A study on climate change pattern of the middle Holocene in Xundian, Yunnan. Trop. Geogr. 29, 515–519 (in Chinese).
Zhang, J.H., Kong, Z.C., 1999. Study on vegetation and climate changes in Beijing region since late Pleistocene. Chin. Geogr. Sci. 9, 243–249.
Zhang, M.L., Yuan, D.X., Lin, Y.S., Qin, J.M., Zhang, C., Cheng, H., 2003. High resolution climatic records of stalagmite from Xiangshui Cave in Guilin since 6.00 ka B P. Acta Geosci. Sin. 24, 439–444 (in Chinese).
Zhang, M.L., Cheng, H., Lin, Y.S., Qin, J.M., Zhang, H.L., Tu, L.L., Wang, H., Feng, Y.M., 2004. High resolution paleoclimatic environment records from a stalagmite of Dongge Cave since 15 000 a in Libo, Guizhou Province, China. Geochimica 33, 65–74 (in Chinese).
Zhang, Q., Sundqvist, H.S., Moberg, A., Körnich, H., Nilsson, J., Holmgren, K., 2010. Climate change between the mid and late Holocene in northern high latitudes – part 2: model–data comparisons. Clim. Past 6, 609–626.
Zhao, H.Y., Leng, X.T., Wang, S.Z., 2002. Distribution, accumulation rate of peat in the Changbaishan Mountains and climate change in Holocene. J. Mountain Sci. 20, 513–518 (in Chinese).
Zhao, Y., Braconnot, P., Marti, O., Harrison, S.P., Hewitt, C., Kitoh, A., Liu, Z., Mikolajewicz, U., Otto-Bliesner, B., Weber, S.L., 2005. A multi-model analysis of the role of the ocean on the African and Indian monsoon during the mid-Holocene. Clim. Dyn. 25, 777–800.
Zhao, Y., Harrison, S.P., 2012. Mid-Holocene monsoons: a multi-model analysis of the inter-hemispheric differences in the responses to orbital forcing and ocean feedbacks. Clim. Dyn. 39, 1457–1487.
Zheng, W., Yu, Y., 2009. The Asian monsoon system of the mid-Holocene simulated by a coupled GCM. Quat. Sci. 29, 1135–1145 (in Chinese).
Zheng, Y.Q., Yu, G., Wang, S.M., Xue, B., Zhuo, D.Q., Zeng, X.M., Liu, H.Q., 2004. Simulation of paleoclimate over East Asia at 6 ka BP and 21 ka BP by a regional climate model. Clim. Dyn. 23, 513–529.
Zhong, W., Shu, Q., 2001. Palaeoclimatic and palaeohydrologic oscillations since about 12.0 ka B.P. at Bosten Lake, southern Xinjiang. Oceanol. Limnol. Sin. 32, 213–220 (in Chinese).
Zhou, B., Zhao, P., 2010. Modeling variations of summer upper tropospheric temperature and associated climate over the Asian Pacific region during the mid-Holocene. J. Geophys. Res. 115, D20109. http://dx.doi.org/10.1029/2010JD014029.
Zhou, J., Wang, S.M., Lü, J., 2003. Climatic and environmental changes from the sediment record of Erhai Lake over the past 10000 years. J. Lake Sci. 15, 104–111 (in Chinese).
Zhou, W.J., An, Z.S., Head, M.J., 1994. Stratigraphic division of Holocene loess in China. Radiocarbon 36, 37–45.
Zhou, W.J., Yu, X.F., Jull, A.J.T., Burr, G., Xiao, J.Y., Lu, X.F., Xian, F., 2004. High-resolution evidence from southern China of an early Holocene optimum and a mid-Holocene dry event during the past 18,000 years. Quat. Res. 62, 39–48.
Zhou, Y.L., Lu, H.Y., Mason, J., Miao, X.D., Swinehart, J., Goble, R., 2008. Optically stimulated luminescence dating of aeolian sand in the Otindag dune field and Holocene climate change. Sci. China Earth Sci. 51, 837–947.